ACSNANO

www.acsnano.org

ARTICLE

Cationic Amphiphilic Drugs Boost the Lysosomal Escape of Small Nucleic Acid Therapeutics in a Nanocarrier-Dependent Manner

Thijs Van de Vyver, Bram Bogaert, Lynn De Backer, Freya Joris, Roberta Guagliardo, Jelter Van Hoeck, Pieterjan Merckx, Serge Van Calenbergh, Srinivas Ramishetti, Dan Peer, Katrien Remaut, Stefaan C. De Smedt, and Koen Raemdonck*

Cite This: *ACS Nano* 2020, 14, 4774–4791

Read Online

ACCESS | Metrics & More | Article Recommendations | Supporting Information

ABSTRACT: Small nucleic acid (NA) therapeutics, such as small interfering RNA (siRNA), are generally formulated in nanoparticles (NPs) to overcome the multiple extra- and intracellular barriers upon *in vivo* administration. Interaction with target cells typically triggers endocytosis and sequesters the NPs in endosomes, thus hampering the pharmacological activity of the encapsulated siRNAs that occurs in the cytosol. Unfortunately, for most state-of-the-art NPs, endosomal escape is largely inefficient. As a result, the bulk of the endocytosed NA drug is rapidly trafficked toward the degradative lysosomes that are considered as a dead end for siRNA nanomedicines. In contrast to this paradigm, we recently reported that cationic amphiphilic drugs (CADs) could strongly promote functional siRNA delivery from the endolysosomal compartment *via* transient induction of lysosomal membrane permeabilization. However, many questions still remain regarding the broader applicability of such a CAD adjuvant effect on NA delivery. Here, we report a drug repurposing screen (National Institutes of Health Clinical Collection) that allowed identification of 56 CAD adjuvants. We furthermore demonstrate that the CAD adjuvant effect is dependent on the type of nanocarrier, with NPs that generate an appropriate pool of decomplexed siRNA in the endolysosomal compartment being most susceptible to CAD-promoted gene silencing. Finally, the CAD adjuvant effect was verified on human ovarian cancer cells and for antisense oligonucleotides. In conclusion, this study strongly expands our current knowledge on how CADs increase the cytosolic release of small NAs, providing relevant insights to more rationally combine CAD adjuvants with NA-loaded NPs for future therapeutic applications.

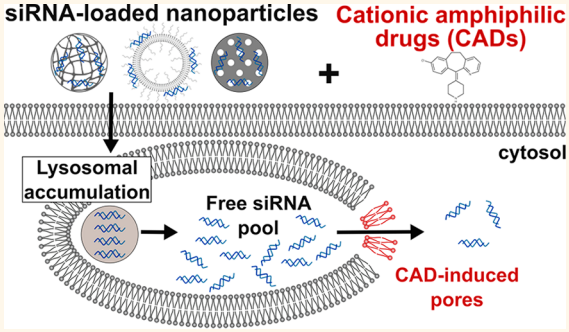

KEYWORDS: *drug repurposing, cationic amphiphilic drugs, lysosomal membrane permeabilization, nucleic acid therapeutics, cellular delivery, endosomal escape, lipid nanoparticles*

Small noncoding RNAs, such as small interfering RNA (siRNA), show great potential for the treatment of a myriad of diseases for which no suitable cure exists to date. Their main mode of action involves post-transcriptional sequence-specific gene silencing, permitting virtually any human pathology with a recognized (over)expression of a disease-causing protein to be addressed.[1−3] To overcome the multiple extra- and intracellular barriers upon *in vivo* administration, nucleic acid (NA) drugs are generally encapsulated into nanoparticles (NPs).[1,4,5] At the cellular level, NPs foster intracellular uptake of NAs by target cells through endocytosis, sequestering them in endosomes.[4−6] However, to exert their gene-silencing function, NAs have to be released from the endosomal lumen into the cytosol.[1,6] Unfortunately, despite the development of multiple endosomal escape strategies (*e.g.*, based on endosomal membrane fusion or disruption), this process remains largely inefficient, with the vast majority of endocytosed drugs being unintentionally routed toward

Received: January 23, 2020
Accepted: April 6, 2020
Published: April 6, 2020

https://dx.doi.org/10.1021/acsnano.0c00666
ACS Nano 2020, 14, 4774–4791

Scheme 1. Cationic Amphiphilic Drugs Enhance the Escape of siRNA from the Lysosomes into the Cytosol[a]

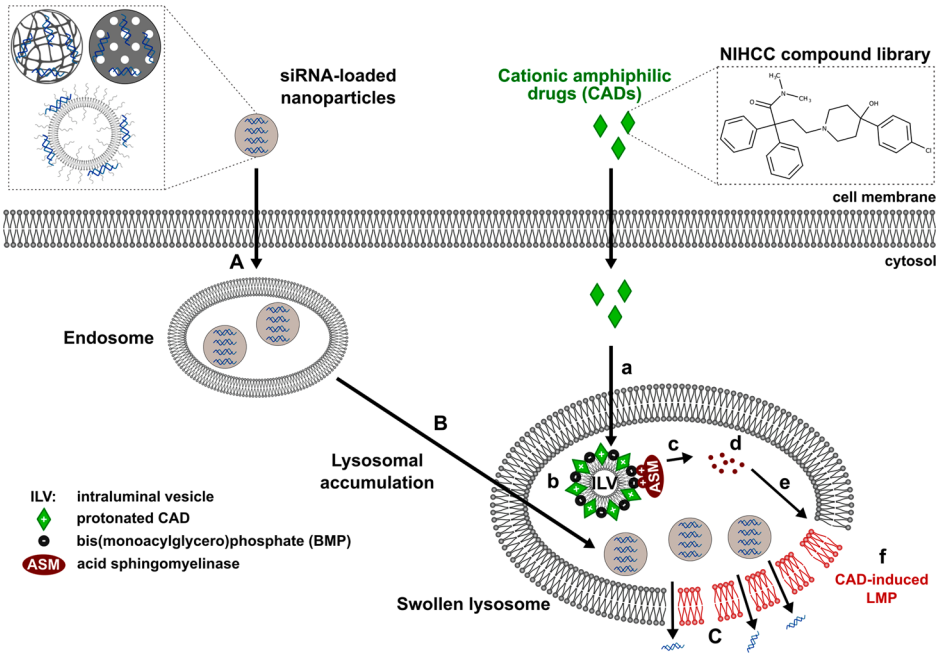

[a]Conditions: (A) Most nanomedicines are internalized by cells *via* an endocytic process and (B) are efficiently routed toward the lysosomal compartment. (C) A CAD-induced transient lysosomal membrane permeabilization (LMP) allows the siRNA molecules to diffuse from the lysosomal lumen into the cytosol. (a) CADs specifically accumulate in lysosomes due to their physicochemical (amphiphilic and weak basic) properties. (b) The cationic lysosomal membrane-associated enzyme acid sphingomyelinase (ASM) is electrostatically bound to the anionic bis(monoacylglycero)phosphate (BMP) lipids of the intraluminal vesicles. (c) Also the CADs become protonated inside the lysosomal lumen, and they insert in intralysosomal membranes, where they induce release of ASM into the lysosomal lumen, followed by (d) its degradation by cathepsins. As the ASM enzyme plays an important role in the lipid homeostasis, functional ASM inhibition leads to (e) lysosomal (phospho)lipidosis (PLD), lysosomal swelling, and (f) a transient LMP.[19]

lysosomes for degradation.[7−12] As a result, typically less than 1% of the internalized NA dose is released into the cytosol.[6−8,13]

Small molecular drugs have proven successful in facilitating (one or more steps) of the intracellular NA delivery process.[14,15,24,16−23] Since the discovery of chloroquine as a small molecule endosomal escape enhancer in 1981, it was only in recent years that other NA delivery enhancers were identified.[14,22−24] Recently, our group demonstrated that lysosomal sequestered siRNA can be released into the cytosol by exposing dextran nanogel-transfected non-small cell lung cancer (NSCLC) cells to selected cationic amphiphilic drugs (CADs).[19] Due to their physicochemical properties, these drugs tend to accumulate inside the acidified lysosomal compartment where they functionally inhibit the acid sphingomyelinase (ASM) enzyme. ASM inhibition leads to a lysosomal storage disease phenotype characterized by phospholipidosis (PLD), lysosomal swelling, and transient lysosomal membrane permeabilization (LMP), allowing the siRNA molecules to diffuse from the lysosomal lumen into the cytosol (Scheme 1).[19] The siRNA-loaded dextran nanogels were used as model NPs in this study, as they have previously shown both a high loading capacity for siRNA as well as feasible cellular uptake, lysosomal accumulation, and gene-silencing efficiency in various cancer cells.[9,19,25−28] These data suggest that, in contrast to general belief, lysosomes should not be considered *per se* as a dead end for siRNA nanomedicines.

As many CADs are widely used (*e.g.*, antihistamines, antidepressants,...) and have a well-documented safety profile, their repurposing as NA delivery enhancers could foster clinical translation of NA drugs. However, many questions still remain regarding the broader applicability of CADs as adjuvants for NA delivery. On the one hand, only a limited number of CADs have been evaluated to date, raising the question if also other CADs share this adjuvant effect. Here, a drug repurposing screen was performed by applying the "National Institutes of Health Clinical Collection" compound library (NIHCC) on the previously reported NSCLC cell model.[19] Additionally, it was investigated if the CAD adjuvant effect can also be extended to other nanocarrier types, including cationic mesoporous silica nanoparticles (MSNPs), (PEGylated) cationic liposomes (LIP), and lipid nanoparticles (LNPs) containing the ionizable lipid DLin-MC3-DMA.[29] Finally, we evaluated if the CADs, besides RNAi-based therapeutics, could also improve the cytosolic delivery of chemically modified antisense oligonucleotides (ASOs) in NSCLC cancer cells, and we confirmed the adjuvant effect of the CADs on a human ovarian SKOV-3 and cervical HeLa cancer cell line. Our data indicate that a multitude of CADs can promote cellular delivery of both siRNAs and ASOs. Importantly, we discovered that the extent of NP internalization by target cells as well as the efficiency of NA decomplexation dictate the success of CAD-promoted endolysosomal escape. Indeed, our data suggest that a sufficient amount of free siRNA is needed inside the lysosomal lumen (*i.e.*, lysosomal pool of free siRNA) to allow diffusion through the CAD-created lysosomal pores into the cytosol (Scheme 1).

RESULTS AND DISCUSSION

Compound Screen of NIH Clinical Collection on Nanogel-Transfected NSCLC Cells. Our previous work disclosed four CADs with diverging chemical structure and

https://dx.doi.org/10.1021/acsnano.0c00666
ACS Nano 2020, 14, 4774−4791

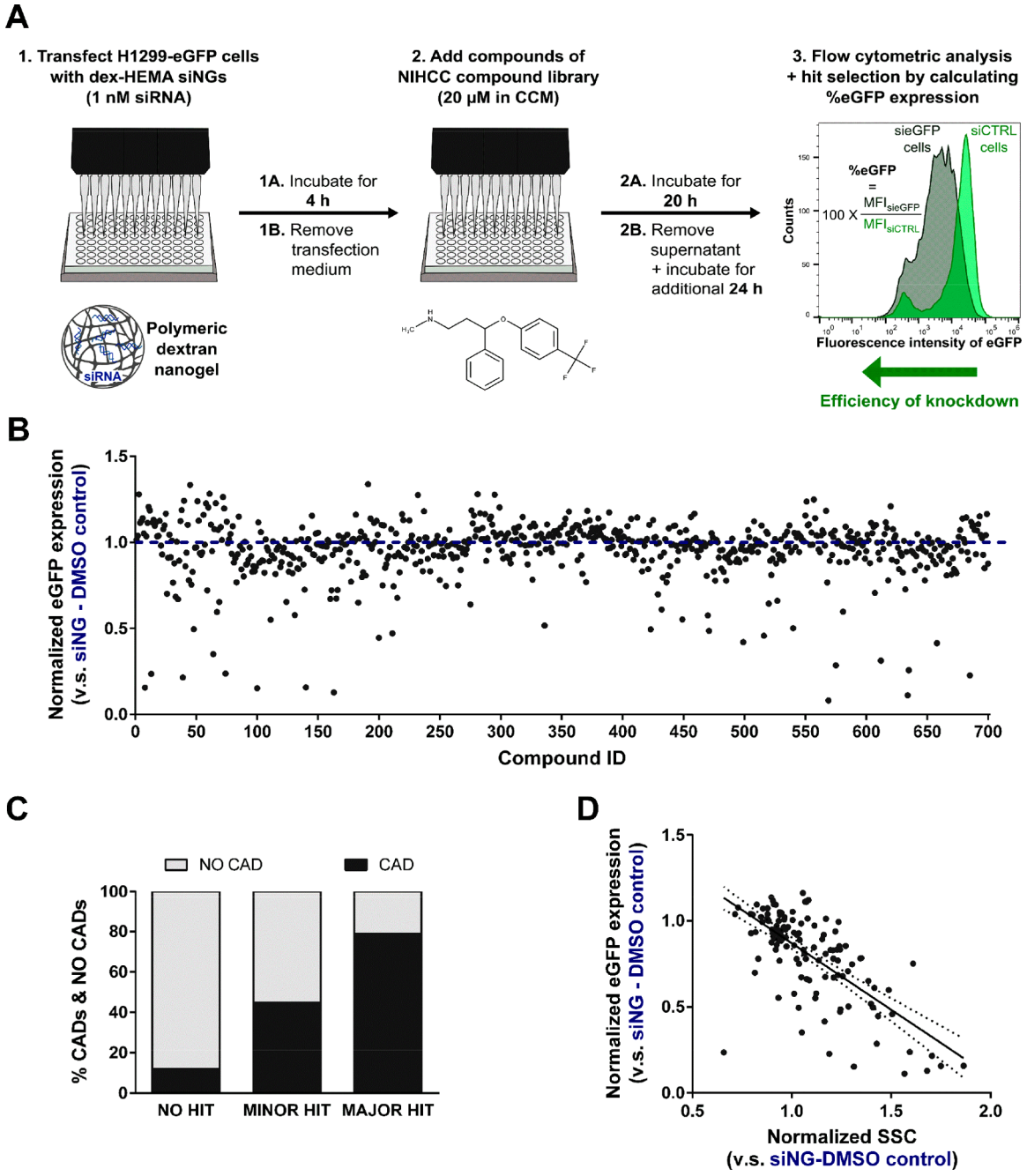

Figure 1. NIHCC compound library identifies multiple CADs as siRNA-delivery promoting compounds. (A) Schematic representation of the protocol used to classify NIHCC compounds as siRNA-delivery-promoting compounds (*i.e.*, "hits"). The CAD fluoxetine is shown as an example of a hit. (B) NIHCC screen summary. The abscissa indicates the number of each compound screened. The ordinate indicates the sequential adjuvant effect of the screened compounds on the eGFP gene-silencing potential of dex-HEMA siNGs (compound concentration = 20 μM, 20 h incubation). The calculated percent eGFP expression values of the individual compounds are normalized to the siNG transfection alone (siNG-DMSO control) of each plate. (C) Fraction of cationic amphiphilic drugs (CADs, clog*P* > 3, and pK_{a1} > 6) in the "no hit", "minor hit", and "major hit" group. (D) Correlation between the SSC signal, normalized to the siNG-DMSO control of each plate, and the normalized eGFP expression (see above) in the group of CADs (n = 128). The dashed line represents the 95% confidence band of the regression line (R^2 = 0.478; p < 0.0001) (eGFP = enhanced green fluorescent protein, NG = dex-HEMA nanogels, siNG = siRNA-loaded NG, NIHCC = National Institutes of Health Clinical Collection, CAD = cationic amphiphilic drug, CCM = complete cell culture medium, siNG-DMSO control = "siNG transfection alone" with equal amount of DMSO, SSC = side scatter, MFI_{siCTRL} = mean fluorescence intensity of the H1299-eGFP cells transfected with siCTRL-loaded NGs, MFI_{sieGFP} = mean fluorescence intensity of the H1299-eGFP cells transfected with sieGFP-loaded NGs).

pharmacology (*i.e.*, nortriptyline, salmeterol, carvedilol, and desloratadine) as siRNA delivery enhancers when applied in a sequential manner to siRNA-transfected cells.[19] To identify additional CADs with an adjuvant effect on the gene-silencing potential of siRNA-loaded dex-HEMA nanogels (dex-HEMA siNGs) in NSCLC cells, we screened the NIHCC (700 compounds) (Figure 1A,B). A sequential (post)treatment protocol with the compounds was used in these experiments, as preincubation was not able to promote gene knockdown (Figure S1A), despite clear indication that the applied CAD (*in*

https://dx.doi.org/10.1021/acsnano.0c00666
ACS Nano 2020, 14, 4774−4791

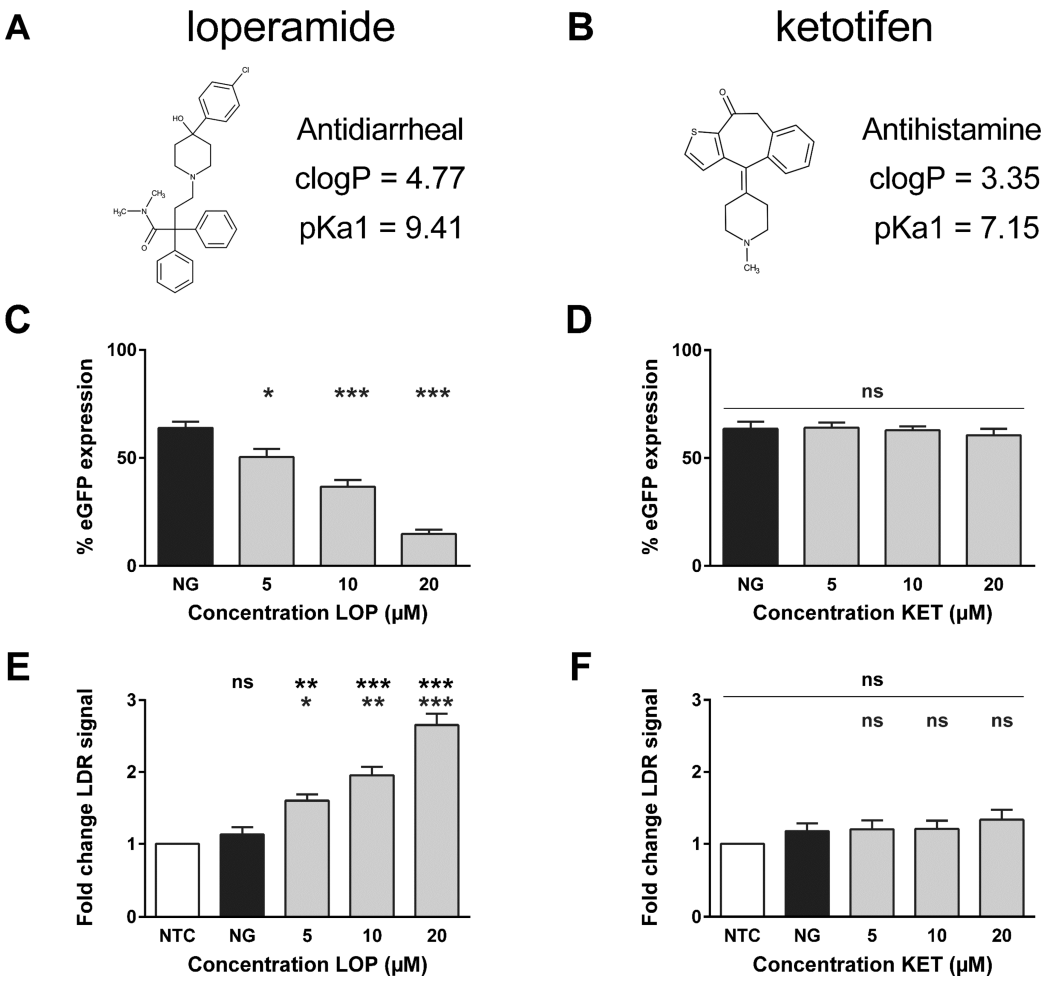

Figure 2. Loperamide, but not ketotifen, improves the eGFP silencing potential of dex-HEMA siNGs in NSCLC cells. (A,B) Drug class, *clogP*, pK_{a1} values, and molecular structure of LOP and KET.[60] The pK_{a1} and *clogP* values of the compounds were predicted with JChem for Office (version 17.21.0.1797, ChemAxon Ltd., Budapest, Hungary).[60] (C,D) Sequential treatment of siNG-transfected H1299-eGFP cells (1 nM siRNA) with "CAD-hit" LOP caused significant additional eGFP silencing in a concentration-dependent manner, whereas "CAD-no hit" KET had no effect at all tested concentrations. (E,F) Fold change in LDR signal, measured *via* flow cytometry, for H1299-eGFP cells sequentially transfected with dex-HEMA siNGs and treated with mounting concentrations of LOP or KET. Data are represented as mean ± the standard error of the mean for minimum three independent repeats. Statistical significance is indicated when appropriate, in black * when referring to the untreated control, and in gray * when compared to dex-HEMA siNG transfection alone (ns, $p > 0.05$, *$p \leq 0.05$, **$p \leq 0.01$, ***$p \leq 0.001$) (*clogP* = calculated log*P*, pK_{a1} = pK_a of the most basic amine, eGFP = enhanced green fluorescent protein, NG = dex-HEMA siNG transfection without sequential CAD treatment, NTC = not treated control, KET = ketotifen, LOP = loperamide, ns = not significant, LDR = LysoTracker Deep Red).

casu desloratadine (DES)) evoked the anticipated lysosomal swelling (Figure S1B). Applying DES immediately after (post) or 20 h after transfection (20 h post) equally promoted the siNG-mediated enhanced green fluorescent protein (eGFP) knockdown. Given the lysosomal accumulation of siNGs demonstrated in earlier work and as CADs are described as lysosomotropic drugs, these results suggest that functional siRNA release mainly occurs from the lysosomal compartment.[9,30] Although we previously showed that a 2 h DES exposure is sufficient to promote siRNA delivery, a 20 h compound treatment was used in this screen, as the lysosomal accumulation kinetics are influenced by the compound's physicochemical properties.[19,31] "Minor" and "major" hit compounds were defined as compounds that significantly promote siNG-mediated eGFP knockdown (*i.e.*, a decrease in % eGFP expression of respectively more than 3 and 6 times the standard deviation on the percent of eGFP expression obtained with the siNG transfection alone, Figure 1A and Figure S2A). Using this protocol, 96 hit compounds that enhance the silencing potential of the siNGs were identified (58 "minor" and 38 "major" hits), with 56 compounds being CADs (calculated log*P* (*clogP*) > 3 and pK_{a1} > 6, Table S1).[32] The high hit rate of 13.7% indicates that physicochemical properties of the compounds may play an important role in the improved siRNA delivery rather than the specific interaction of a compound with a molecular target.[33] Interestingly, the "hit" group was significantly enriched in CADs (Figure 1C, Figure S2E, and Table S1), with diverging chemical structure and pharmacological activity. Many CADs are known as functional inhibitors of the lysosomal acid sphingomyelinase (ASM, FIASMAs) enzyme, which in part explains the concurrent enrichment in both documented ASM inhibitors ("ASMi+", Figure S2B,E) and PLD inducers ("LipidTOX+" and "PLD+", Figure S2C−E).[31,32,34,35] Note that within the CAD group a clear positive correlation was found between the side scatter (SSC) signal, indicative of increased cellular granularity as a

https://dx.doi.org/10.1021/acsnano.0c00666
ACS Nano 2020, 14, 4774−4791

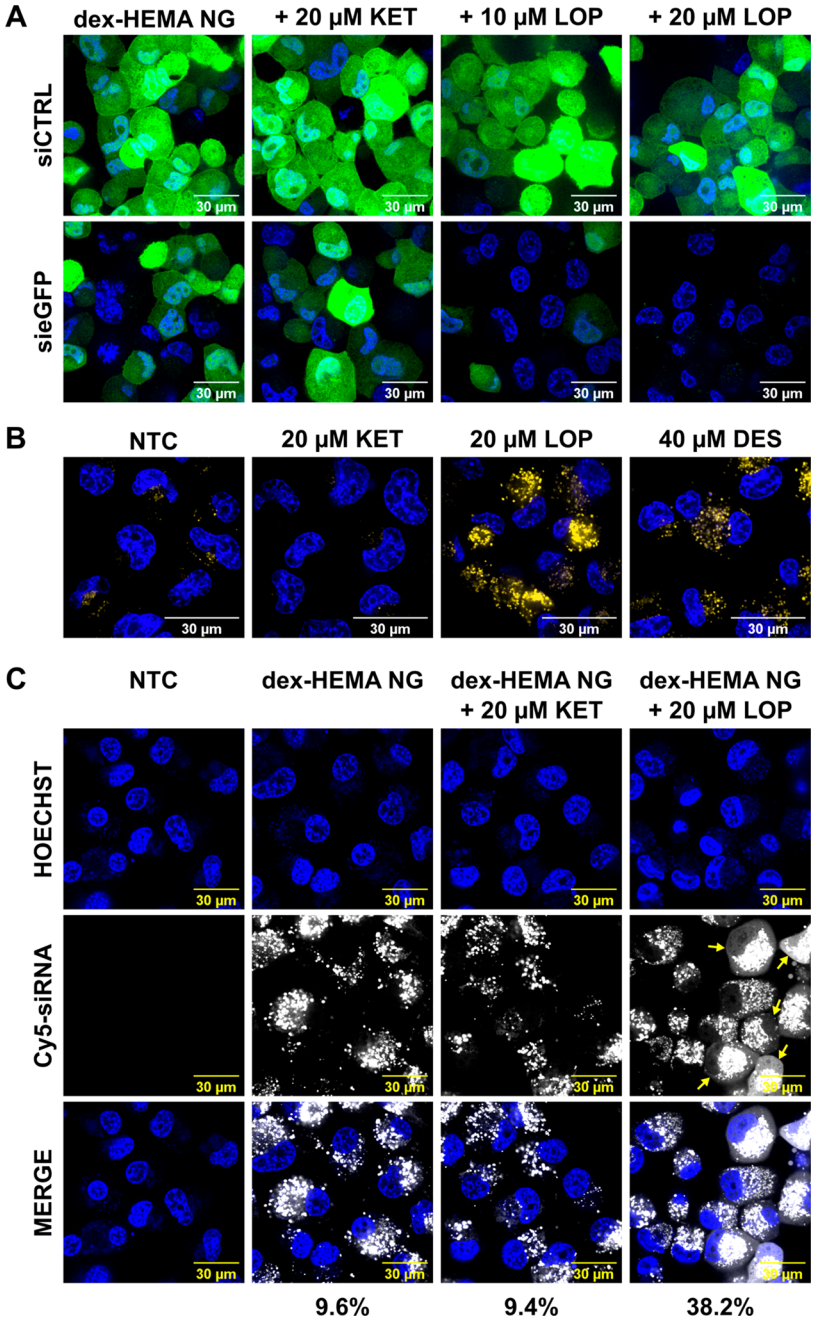

Figure 3. Loperamide, but not ketotifen, induces a phospholipidosis phenotype and promotes siRNA release into the cytosol. (A) Representative confocal images from the eGFP expression of H1299-eGFP cells after transfection with dex-HEMA NGs loaded with a suboptimal amount of siCTRL or sieGFP (2 nM), whether or not followed by treatment with 20 μM KET or 10−20 μM LOP for 20 h. (B) Representative confocal images from the phospholipid distribution in H1299-eGFP cells visualized with LipidTOX Red PLD detection reagent in untreated and 20 μM KET/20 μM LOP/40 μM DES treated cells (20 h). (C) Representative confocal images from the intracellular siCy5 distribution in H1299-WT cells, only transfected with siCy5-loaded dex-HEMA NGs, or cells subsequently incubated with 20 μM KET or LOP for 20 h. The values below the images correspond to the percentage of cells with a diffuse cytosolic siCy5 signal. Cells with a diffusive siCy5 signal are shown with yellow arrows. The scale bar corresponds to 30 μm (NTC = not treated control, NG = nanogels, siCTRL = siRNA scrambled control, sieGFP = siRNA targeting eGFP, eGFP = enhanced green fluorescent protein, KET = ketotifen, LOP = loperamide, DES = desloratadine).

result of lysosomal swelling and the siNG-mediated knockdown (Figure 1D).[19] Moreover, the CADs in the hit group have a higher *clogP* (4.49 ± 1.08) compared to that of the CAD-no hit group (3.94 ± 0.73), whereas the pK_{a1} value was not significantly different (Figure S2G). This result suggests that the siRNA delivery-promoting effect is dependent on the degree of lysosomal accumulation and membrane insertion, which is facilitated by CAD lipophilicity.[31,36,37] Although these data correlate CAD physicochemistry with the induction of an acquired lysosomal storage disease phenotype and improved siRNA delivery (Figure 1D), 72 of the 128 CADs (~56%) present in the screen were not identified as adjuvants at 20 μM (Figure S2E,F), which corroborates earlier findings by us and others that not all CADs are FIASMAs, induce LMP, or are

https://dx.doi.org/10.1021/acsnano.0c00666
ACS Nano 2020, 14, 4774−4791

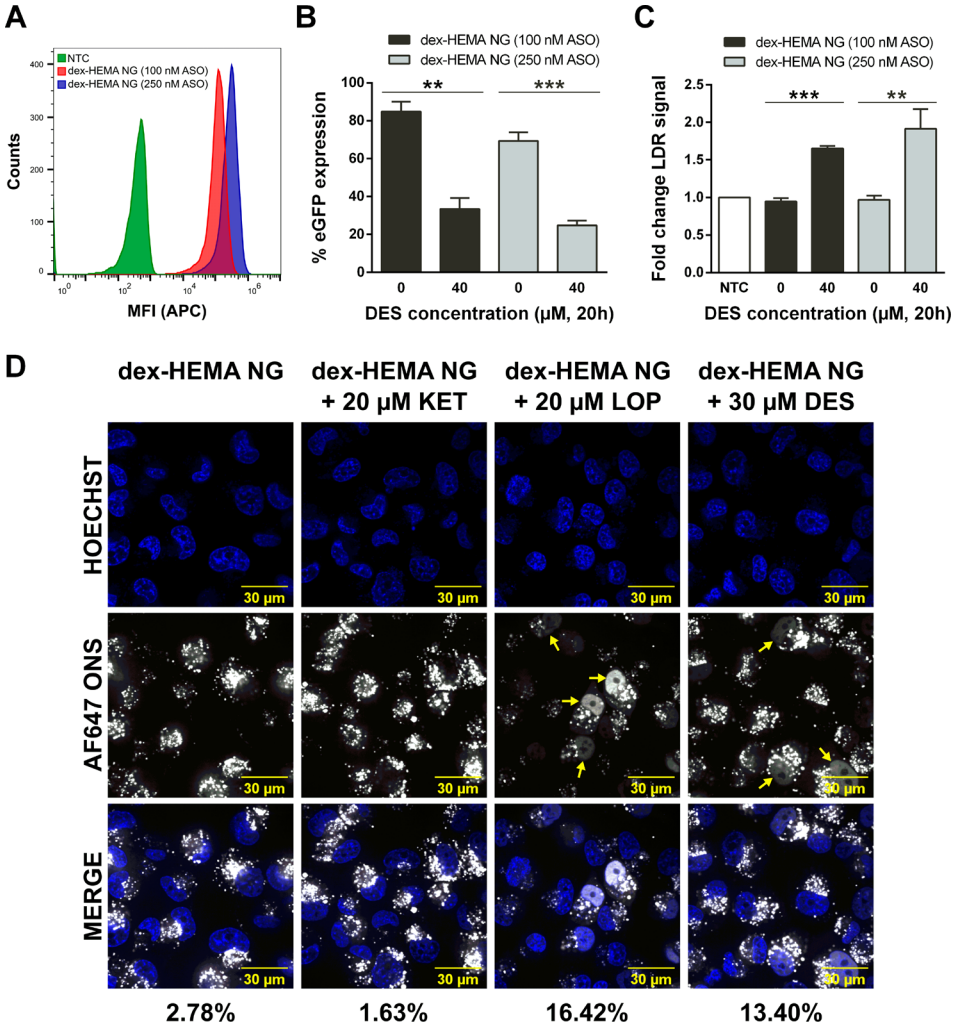

Figure 4. CADs enhance the delivery of ASOs/ONs in NSCLC cells. (A) Evaluation of cellular uptake of dex-HEMA ASO-NGs, loaded with suboptimal amounts of Cy5-labeled ASOs, in H1299-eGFP cells determined *via* flow cytometry. (B) eGFP silencing in H1299-eGFP cells with dex-HEMA ASO-NGs could be significantly improved through sequential treatment with 40 μM DES for 20 h. (C) Fold change in LDR signal, measured *via* flow cytometry, for H1299-eGFP cells sequentially transfected with dex-HEMA ASO-NGs and treated with 40 μM DES for 20 h. (D) Representative confocal images from the intracellular AF647 ON distribution in H1299-eGFP cells, only transfected with AF647 ON-loaded dex-HEMA NGs, or cells subsequently incubated with 20 μM KET/20 μM LOP/30 μM DES for 20 h. Nuclei can be seen in blue, and cells in which escape happened show nuclear fluorescence in the red channel (red fluorescence is depicted white) due to the release of AF647 ONs in the cytosol. The values below the images correspond to the percentage of cells with white nuclei (yellow arrows). The scale bar corresponds to 30 μm. Data are represented as mean ± the standard error of the mean for minimum three independent repeats. Statistical significance is indicated when appropriate, in black * when referring to ASO-NG transfection alone (100 nM ASO), and in gray * when compared to ASO-NG transfection alone (250 nM ASO) ($p \leq 0.01$, ***$p \leq 0.001$) (CADs = cationic amphiphilic drugs, ASO = phosphorothioate gapmer antisense oligonucleotide, NTC = not treated control, NG = nanogels, DES = desloratadine, LDR = LysoTracker Deep Red, MFI = mean fluorescence intensity, APC = allophycocyanin (red channel), ON = oligonucleotide, AF647 = AlexaFluor647 dye).**

active in the same dose range.[19,31,38−41] "Cationic amphiphilic drugs" is considered an umbrella term for a class of pharmacologically and structurally very diverse compounds. As all compounds were added to the cells in serum-containing cell culture medium, differences in structure and physicochemical properties between the various CADs will affect protein binding and final endolysosomal concentration.[42−49] Previous compound screens have likewise shown that the presence of serum in the incubation medium can influence a molecule's cellular activity.[50,51] In addition, it is conceivable that structural differences will also impact the efficiency with which the CADs insert in lysosomal membranes and induce an acquired lysosomal storage disease phenotype.[52] Indeed, a recent study by Rhein *et al.* showed that subtle modifications of the structures of the CADs imipramine and desipramine (both "CAD-hits" in our study, Table S1) could markedly change their ability to inhibit ASM and induce PLD.[53] To investigate whether distinctive structural components could be unveiled in the various groups ("hits", "no hits", "CAD-hits", "CAD-no hits"), the structures of all 700 NIHCC compounds were analyzed using a Web-based principal component analysis (PCA) tool that projects Morgan fingerprints, which are representations of the chemical structures of the compounds, into new sets of coordinates (PC1 and PC2; Figure S2F).[54] The "CAD-hits" being randomly distributed across the PCA scatter plots suggests that the chemical diversity of the "CAD-hits" is not substantially different from the CADs that were not identified as hits. However, a more detailed structure−activity relationship falls

https://dx.doi.org/10.1021/acsnano.0c00666
ACS Nano 2020, 14, 4774−4791

beyond the scope of this article. Although our data strongly suggest that the CAD-induced LMP is a consequence of the functional inhibition of ASM, we cannot rule out the possibility that CADs might promote siRNA delivery *via* one or more alternative mechanisms. These could include proteolysis of other lysosomal lipases (*e.g.*, acid ceramidase) and the ability of certain CADs to induce a direct detergent effect or to enhance reactive oxygen species (ROS) production.[39,55] The extent to which these additional effects take place are likely different for each CAD, making an unambiguous correlation between CAD adjuvant effect and CAD-induced ASM inhibition especially difficult.

Most importantly, this compound screen highlights that the observed adjuvant effect on siRNA delivery is not limited to the previously identified CAD molecules (*i.e.*, nortriptyline, carvedilol, salmeterol, and DES), but that many more physicochemical related compounds phenocopy these effects.[19]

Secondary Validation of the CADs Ketotifen and Loperamide. As mentioned above, not all CADs emerged as hits in our primary screen. To validate this finding, two CADs were selected for secondary testing. As shown in Table S1, loperamide (LOP, Figure 2A) is a "CAD-hit", whereas ketotifen (KET, Figure 2B) has the physicochemical properties of a CAD but was not identified as a hit (not shown in Table S1). Although LOP evoked a concentration-dependent increase in (a) eGFP silencing (Figure 2C), (b) lysosomal volume (Figure 2E), and (c) cellular granularity (Figure S3A) compared to untreated and dex-HEMA siNG-transfected cells, exposure of the cells to mounting concentrations of KET could not replicate these effects (Figure 2D,F and Figure S3B). The contrasting effect of both compounds on dex-HEMA siNG-induced eGFP silencing was also visually confirmed with confocal microscopy (Figure 3A). In addition, staining of CAD-treated cells with the PLD detection reagent LipidTOX Red (Figure 3B and Figure S4A) revealed that 20 μM LOP treatment induced an accumulation of lipids in vesicular structures, whereas the same concentration of KET did not. In line with previously documented data on the functional inhibition of ASM, LOP-treated H1299-WT cells (as well as cells treated with 6 other "CAD-hit" compounds) also showed a higher green fluorescent signal when stained overnight with BODIPY FL C12-sphingomyelin, in contrast to 20 μM KET treatment (Figure S4B), which indicates reduced sphingomyelin degradation due to ASM inhibition.[56−59] Similarly, only LOP exposure could visually increase the cytosolic delivery of Cy5-labeled siRNA, as evident from Figure 3C. Upon treatment with 20 μM LOP, ∼38% of the cells showed a diffuse cytosolic siRNA fluorescence in contrast to the untreated and KET-exposed cells where a punctate pattern, indicative of lysosomal sequestration, was observed. Note that the percentage of cells that showed cytosolic delivery of fluorescent siRNA is lower than was expected based on the eGFP gene-silencing results (Figure 2C,D and Figure 3A), which can be most likely attributed to the cytosolic dilution of the labeled siRNAs below the detection limit of a standard confocal microscope.[7,19] Of note, the tested CADs were overall well tolerated in the applied concentrations (Figure S4C), in line with our previously reported data.[19] It should, however, be noted that not all "CAD-hits" shown in Table S1 have been routinely tested for their impact on cell viability. In summary, the effects of the "CAD-hit" LOP and the "CAD-no hit" KET on gene knockdown and lysosomal phenotype could be validated.

Confirmation of the CAD Adjuvant Effect on a Different Cargo and Cell Model. Although chemically stabilized gapmer antisense oligonucleotides (∼6 kDa) are single-stranded NAs with a different mode of action for mRNA cleavage compared to double-stranded siRNAs, they face similar intracellular delivery challenges.[1,61,62] Hence, the effect of the previously identified CAD adjuvant DES on the eGFP gene-silencing potential of dex-HEMA NGs loaded with an eGFP-targeting ASO (eGFP-ASO) was examined.[19] Note that DES, the main compound tested in our earlier work, was confirmed in the NIHCC screen as one of the most promising hits ("major" hit, Table S1). Keeping clinical translation in mind, antihistamines like DES may provide a safer alternative compared to antipsychotics or compounds targeting opioid receptors. Hence, we mainly used DES to assess the broader applicability of the CAD adjuvant approach in this article. The ASO-loaded dex-HEMA NGs (ASO-NG) were efficiently internalized by the H1299-eGFP cells (Figure 4A), and both tested ASO concentrations induced a suboptimal eGFP knockdown (Figure 4B). Sequential treatment with 40 μM DES, the most effective concentration for this compound,[19] clearly promoted ASO-NG gene silencing (Figure 4B), which coincided with a marked enlargement of the total lysosomal volume (Figure 4C). Visual microscopic confirmation of the enhanced cytosolic oligonucleotide delivery by DES and LOP adjuvant treatment was obtained with AlexaFluor647-labeled oligonucleotides (AF647 ONs), which upon endosomal egress migrate to the cell nucleus (Figure 4D). A punctate pattern was observed for the majority of untreated and 20 μM KET-treated cells, indicating lysosomal sequestration, whereas 20 μM LOP and 30 μM DES clearly increased the amount of stained nuclei (Figure 4D). Also, the percentage of cells that showed cytosolic ON delivery is relatively low, which likely can again be attributed to the cytosolic dilution of the labeled ONs.[7,19] Whereas gapmer ASOs induce RNase H1 cleavage of the target mRNA, siRNAs make use of the endogenous RNAi machinery.[3,12] The enhanced ASO-mediated eGFP knockdown upon DES exposure thus proves that the enhanced silencing effect is independent of the RNAi pathway but likely results from improved cytosolic delivery.

Next, we also quantified the adjuvant effect of two CAD-hits (*i.e.*, DES and salmeterol (SAL)) on dex-HEMA siNG-induced luciferase silencing in a SKOV-3-LUC+ cell line that stably expresses the firefly luciferase protein (Figure S5). Similar to the experiments with the H1299-eGFP cells, the siNGs were efficiently internalized (Figure S5A), and a sequential 20 h drug treatment with SAL or DES strongly enhanced the luciferase silencing in a concentration-dependent manner (Figure S5B−D). Comparable results were seen for the SKOV-3-LUC2 IP2 (20 h incubation) and HeLa NLS-GFP (2 h incubation) cell line (Figure S7H,I). Finally, enhanced endolysosomal escape of AF647 ONs could be visualized in SKOV-3-LUC2 IP2 cells for 30 μM DES, 30 μM SAL, and 20 μM LOP but not 20 μM KET (Figures S6 and S7A−G). In conclusion, next to the NSCLC cell model we could confirm the CAD adjuvant effect for siRNA and/or oligonucleotide delivery on a luciferase expressing SKOV-3 cell line and a HeLa cell line.

Evaluation of CAD Adjuvant Effect on Different siRNA-Loaded Nanocarriers. Next to the biodegradable dex-HEMA siNGs used above, also many other NPs are internalized by cells *via* an endocytic process and efficiently routed toward the lysosomal compartment.[7−11,30,63−65] Here, we evaluated if the CAD adjuvant approach could similarly improve the cytosolic siRNA delivery of a panel of siRNA-loaded NPs: that is, nonbiodegradable polymeric dextran NGs (dex-MA),[9,26]

https://dx.doi.org/10.1021/acsnano.0c00666
ACS Nano 2020, 14, 4774−4791

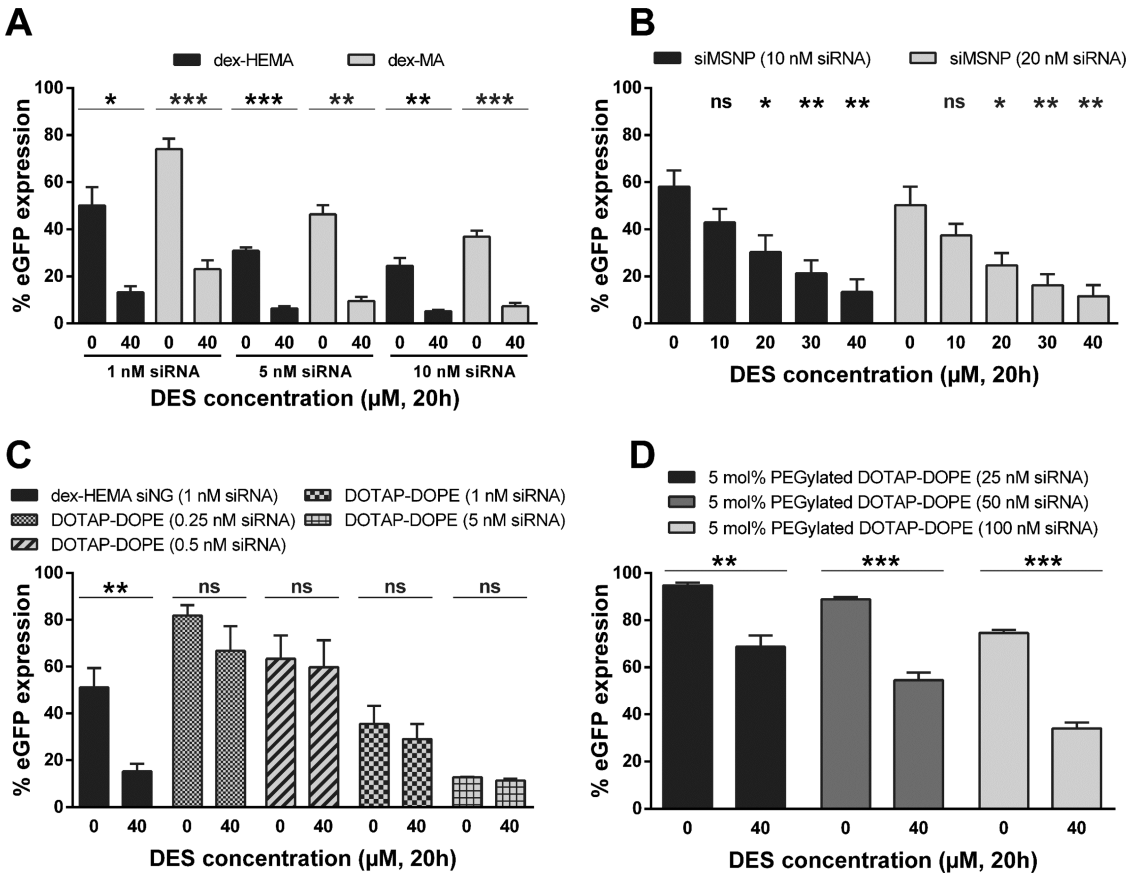

Figure 5. Adjuvant effect of desloratadine on eGFP silencing in H1299-eGFP cells is nanocarrier-dependent. (A–D) Influence of 20 h sequential adjuvant treatment with DES on the transfection efficiency of dex-(HE)MA siNGs, siMSNPs, or (PEGylated) DOTAP-DOPE siLIP. Data are represented as mean ± the standard error of the mean for minimum three independent repeats. Statistical significance is indicated when appropriate, in black * when referring to dex-HEMA siNG, PEGylated DOTAP-DOPE siLIP, or siMSNP (10 nM siRNA) transfection alone, and in gray * when compared to dex-MA siNG, DOTAP-DOPE siLIP, or siMSNP (20 nM siRNA) transfection alone (ns, $p > 0.05$, *$p \leq 0.05$, **$p \leq 0.01$, ***$p \leq 0.001$) (siNG = siRNA-loaded nanogel, siLIP = siRNA-loaded liposomes, DES = desloratadine, ns = not significant, siMSNP = siRNA-loaded propylamine-functionalized mesoporous silica nanoparticle).

inorganic propylamine-functionalized MSNPs, cationic LNPs, such as (PEGylated) DOTAP-DOPE liposomes, the lipofection reagent Lipofectamine RNAiMAX (LF RNAiMAX), and lipid nanoparticles containing the ionizable lipid DLin-MC3-DMA (MC3 LNPs) in H1299-eGFP cells (Scheme S1). The physicochemical properties of the (PEGylated) DOTAP-DOPE LIP and the MC3 siLNPs are shown in Figures S10 and S11. A sequential 20 h incubation with 40 μM DES, a previously identified adjuvant that also emerged as a major CAD-hit in the NIHCC screen, was used as CAD treatment to ensure clear induction of the anticipated lysosomal phenotype.[19]

Although lower eGFP silencing was observed for the stable dex-MA siNGs compared to their degradable dex-HEMA counterparts, sequential DES treatment achieved >90% eGFP knockdown for both particles (Figure 5A). A comparable result was obtained with siRNA-loaded MSNPs (siMSNPs) (Figure 5B). Hence, these data indicate that the CAD adjuvant effect is independent of the intrinsic degradability of the used NGs and can also be effective on inorganic nanocarriers.

In contrast, this CAD adjuvant effect on siRNA delivery could not be observed for the cells transfected with siRNA-loaded cationic LNPs such as DOTAP-DOPE LIP or LF RNAiMAX (Figure 5C and Figure S9A), despite clear indication that the applied DES evoked lysosomal swelling (Figures S8A and S9B). Previous studies by our group and others, evaluating the effect of photochemical internalization (PCI) on siRNA-loaded Lipofectamine RNAiMAX or Lipofectamine 2000, showed comparable results. PCI is a technique that destabilizes endosomal membranes by the application of amphiphilic photosensitizers, which upon photoactivation evoke oxidative endolysosomal membrane damage through the production of ROS.[9,26,66] In line with the observations on CADs, the silencing potential of siRNA-loaded cationic LNPs was unaffected by PCI, whereas the cellular siRNA delivery *via* dex-(HE)MA siNGs was strongly enhanced.[9,26]

As state-of-the-art LNPs are generally PEGylated, the influence of including a PEGylated lipid (DSPE-PEG_{2000}) in the formulation was also probed. Although higher siRNA and LIP concentrations were needed to achieve target gene knockdown compared to the non-PEGylated counterpart, a clear adjuvant effect of DES on the siRNA delivery efficiency could be seen when the DOTAP-DOPE LIPs were modified with 5 mol % of the PEGylated lipid (Figure 5D and Figure S8B). In contrast, DES was not able to improve siRNA delivery mediated by ionizable MC3 siLNPs (Figure S12A,B), despite being PEGylated (1.5 mol % of DMG-PEG_{2000}) and neutrally charged at physiological pH. Given the clear dependency on the type of nanocarrier, we next sought to investigate in more detail which requirements a therapeutic siNP should have to be compatible with the proposed CAD adjuvant approach.

https://dx.doi.org/10.1021/acsnano.0c00666
ACS Nano 2020, 14, 4774–4791

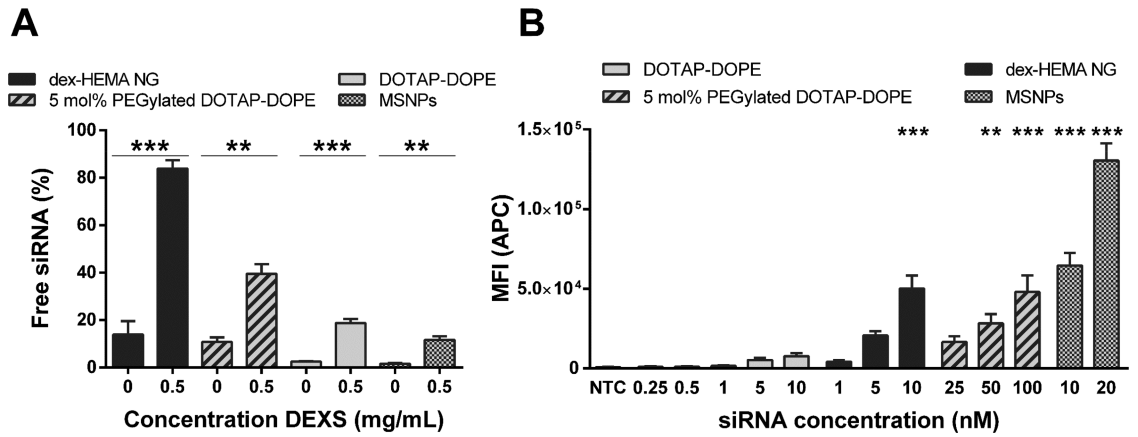

Figure 6. siRNA nanocarrier decomplexation and intracellular siRNA amount. (A) DEXS-induced siRNA release from the indicated siNPs in HEPES buffer (pH 7.4, 20 mM), as measured by fluorescence fluctuation spectroscopy. The concentration of fluorescent siRNA (siCy5) equaled 25 nM in all samples. Data are represented as mean ± the standard error of the mean for minimum three independent repeats. Statistical significance with respect to the 0 mg/mL DEXS condition (black *) is indicated when appropriate ($p \leq 0.01$, ***$p \leq 0.001$). (B) Quantification of cellular uptake of dex-HEMA NGs, MSNPs, and (PEGylated) DOTAP-DOPE LIP (at varying siRNA concentrations) in H1299-eGFP cells determined *via* flow cytometry. Data are represented as mean ± the standard error of the mean for minimum three independent repeats. Statistical significance with respect to the NTC (black *) is indicated when appropriate (**$p \leq 0.01$, ***$p \leq 0.001$) (FFS = fluorescence fluctuation spectroscopy, DEXS = 10 kDa dextran sulfate, NG = nanogel, MSNP = propylamine-functionalized mesoporous silica nanoparticle, NP = nanoparticle, NTC = not treated control, MFI = mean fluorescence intensity, APC = allophycocyanin (red channel)).**

Decomplexation Efficiency and Intracellular siRNA Dose Define Successful CAD−Nanocarrier Combinations. Previous work from our group suggested that the CAD-induced pores in the lysosomal membrane (Scheme 1) are relatively small, only allowing the passage of decomplexed siRNA but not substantially larger NA therapeutics (*e.g.*, mRNA).[19] To probe the size of the CAD-induced pores, we examined the ability of 40 μM DES to improve the cytosolic delivery of FITC-labeled dextrans (FDs) of different molecular weight, which were co-incubated with the MSNPs for 4 h. The confocal images (Figure S13) clearly indicate that the combination of a CAD-responsive NP (MSNPs) and 40 μM DES can release FDs up to 150 kDa in the cytosol, judging from the diffuse cellular FD signal. Of note, the used FD solutions are rather polydisperse mixtures (as indicated by the manufacturer and as previously shown by our group), with the 150 kDa dispersion having a size range of approximately 10−40 nm.[67] As such, these data imply that the actual pore size might be lower than the average 150 kDa size. Although such a pore size is larger than the size of most cell-death-evoking cathepsins (20−30 kDa), no extensive reduction in cell viability is observed (Figure S4C). These results suggest that CADs only trigger minor and nonlethal LMP. Extensive LMP involves a substantial release of lysosomal cathepsins and cytosolic acidification, which would cause uncontrolled cell death. On the contrary, partial LMP might release a limited amount of cathepsins, which are subsequently deactivated by the neutral pH of the cytosol or by the action of endogenous cathepsin inhibitors.[68−70] In addition, components of the endosomal sorting complex required for transport (ESCRT) machinery, such as the ESCRT-III complex, are able to repair permeabilized lysosomal membranes or damaged lysosomes can be routed into the lysophagy pathway.[71,72] Altogether, these data indicate that the DES-created pores exceed the size of a single siRNA duplex (~14 kDa) but not that of siRNA-loaded NPs used in this article (60−200 nm), thus only allowing passive diffusion of the decomplexed fraction of siRNA. We postulate that differences in this free siRNA fraction, which is determined by both the total intracellular dose as well as the siRNA release efficiency from the nanocarrier, could explain why the delivery efficiency of some nanocarriers can be stimulated with CADs while not of others.

Therefore, we first quantified the nanocarrier's susceptibility to siRNA decomplexation with a competing polyanion (10 kDa dextran sulfate (DEXS)) of which the size approximates that of a siRNA duplex.[30,73] Exposure of the different siNPs to DEXS resulted in marked differences in the extent of siRNA decomplexation, with the siNGs and siMSNPs being most and least susceptible to siRNA release, respectively (Figure 6A and Figure S12C). Importantly, also PEGylation of the DOTAP-DOPE LIP led to a higher fraction of free siRNA in the presence of DEXS. A possible explanation for this discrepancy can be found in the impact of PEGylation on the LIP nanoarchitecture. Indeed, siRNA complexation by non-PEGylated cationic liposomes leads to a multilamellar formulation with the majority of the siRNA molecules packed between opposing bilayers. In contrast, the presence of a PEG layer on the liposomal surface prior to siRNA complexation precludes this multilayer buildup, thus leaving the siRNA mostly associated with the liposomal surface (as schematically shown in Figure S10B). This PEG-induced difference in nanoarchitecture could lead to an easier decomplexation (Figure 6A) of the nucleic acid payload in extracellular biofluids as well as inside the cell, as previously shown by our group and others for siRNA, oligonucleotides, and/or pDNA.[74−81] One could expect that a facilitated decomplexation in the endolysosomal compartment increases the likelihood of successful cytosolic influx of siRNA through CAD-induced pores in the limiting endolysosomal membrane. This model is further supported by the data obtained with the MC3 siLNPs. A MC3 formulation prepared *via* microfluidic mixing leads to stable siRNA encapsulation in the LNP core and precludes siRNA decomplexation in the presence of competing polyanions, even at higher DEXS concentrations (Figure S12C).[82−84] This suggests that the fraction of siRNA that is not released into the cytosol *via* fusion of the LNP with the limiting endosomal membrane remains tightly complexed and is not available for CAD-induced lysosomal escape.

https://dx.doi.org/10.1021/acsnano.0c00666
ACS Nano 2020, 14, 4774−4791

Scheme 2. siRNA-Loaded Nanoparticle Transfection Needs to Result in a Lysosomal Pool of Free (Decomplexed) siRNA to Be Responsive to CAD Adjuvant Treatment[a]

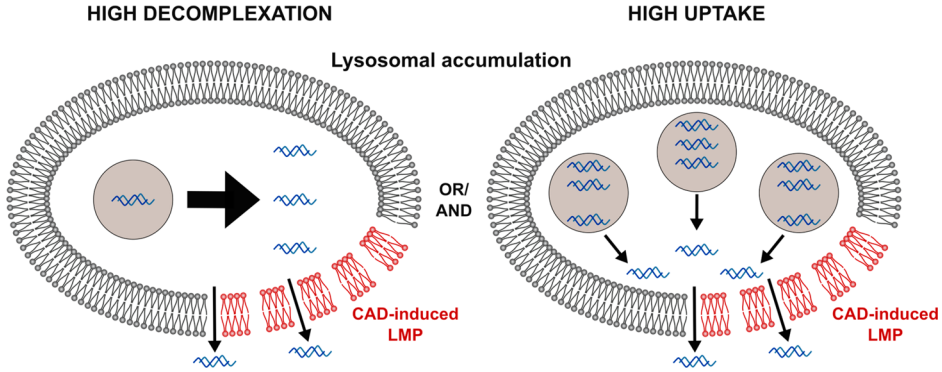

[a]At the used siRNA and NP concentrations, the cellular internalization of the dex-(HE)MA siNGs remains low, but the siRNA is easily decomplexed from the NGs. On the contrary, the siMSNPs are taken up very efficiently, but the siRNA decomplexation remains low. The 5 mol % of PEGylated DOTAP-DOPE siLIP combines features of both the latter NPs (decomplexation and cellular internalization between the siNGs and the siMSNPs). All of these types of NPs subsequently result in a lysosomal pool of free (decomplexed) siRNA, and the CAD molecules can induce extra siRNA release by the formation of small and transient pores in the lysosomal membranes. DOTAP-DOPE siLIP, Lipofectamine RNAiMAX, and MC3 siLNPs are, however, incompatible with the CAD adjuvants, as the siLIP/siLNP uptake remains low while the lysosomally accumulated lipoplexes are also not easily decomplexed (CAD = cationic amphiphilic drug, siLIP = siRNA-loaded liposomes, siNG = siRNA-loaded nanogel, siMSNP = siRNA-loaded propylamine-functionalized mesoporous silica nanoparticle, MC3 siLNPs = siRNA-loaded lipid nanoparticles containing the ionizable lipid DLin-MC3-DMA, NP = nanoparticle, LMP = lysosomal membrane permeabilization).

Second, the cellular uptake of the siNPs was investigated at the siRNA concentrations used for the silencing experiments, which gives an indication of the intracellular siRNA dose at the time of CAD exposure. As evident from Figure 6B, DOTAP-DOPE LIP and dex-HEMA NGs are the most efficient siRNA carriers in contrast to the MSNPs, the latter which require markedly higher intracellular siRNA doses to achieve significant knockdown. As expected, PEGylation decreases the siRNA delivery performance of the DOTAP-DOPE LIP.[79] PEGylated MC3 siLNPs, on the other hand, show an uptake behavior similar to that of the non-PEGylated DOTAP-DOPE LIP, albeit with a marginally lower siRNA delivery efficiency (Figure S12A,D).

In summary, the straightforward siRNA decomplexation observed for the dex-HEMA NGs, in line with previous observations,[30,73] likely correlates with the improved siRNA delivery following CAD exposure (Figure 6A), as we envisioned only the transfer of decomplexed siRNA/ASO molecules to the cytosol. On the other hand, the siMSNPs have a low decomplexation efficiency (Figure 6A), similar to the DOTAP-DOPE siLIP, while the delivery efficiency of the former can still be promoted with sequential CAD treatment (Figure 5B). The explanation for this observation lies in the much higher intracellular siRNA dose introduced by the MSNPs (~80−162 fold), compared to the DOTAP-DOPE LIP (~1.2−1.9 fold) (Figure 6B). Likewise, the much higher intracellular siRNA doses required by PEGylated DOTAP-DOPE LIP to achieve target gene knockdown (Figure 6B) will, in part, account for their CAD responsiveness. MC3 siLNPs obtained *via* rapid microfluidic mixing behave similarly as the DOTAP-DOPE siLIP (Figure S12), as the very stable siRNA encapsulation in the LNP core precludes the observation of a CAD adjuvant effect.

Based on the present results, it is suggested that a lysosomal pool of free (decomplexed) siRNA is needed to obtain a CAD adjuvant effect. This is achieved either by a sufficient siRNA decomplexation, a high extent of NP endocytosis or a combination of both (*i.e.*, dex-HEMA NGs, PEGylated DOTAP-DOPE LIP, and MSNPs), altogether contributing to the intraendosomal fraction of decomplexed siRNA (Scheme 2).

The data shown in this article strongly contribute to our knowledge about the prerequisites a therapeutic siNP should have to be compatible with the proposed CAD adjuvant approach. More specifically, the nanocarrier should be stable in extracellular media, such as the bloodstream, but should easily release the encapsulated siRNA following endocytosis. State-of-the-art MC3 LNPs have demonstrated excellent *in vivo* siRNA delivery performance, but studies have shown that the majority of LNPs also accumulates in the lysosomal compartment, with only a small fraction (1−2%) of siRNAs being able to escape to the cytosol.[7,8,85] Our data indicate that this lysosomal fraction cannot be additionally released by CAD-induced LMP, likely due to too stable siRNA incorporation. Hence, *in vivo* evaluation of CAD-promoted siRNA delivery would require dedicated NP design taking into account the above-mentioned criteria.[73,76,86,87] Also other challenges (*e.g.*, identification of suitable CAD doses) should be taken into account. It has been observed in the literature that CADs, even after oral administration and in therapeutic doses, can block ASM activity and induce LMP *in vivo* in cancer cells.[38,39,88,89] CADs typically have high distribution volumes (*e.g.*, >100 L/kg for DES), facilitating efficient distribution to tissues where *in vivo* PLD induction has been documented, whereas the lower pH in tumors may lead to more efficient accumulation of the weak basic CADs.[35,38] Moreover, transformed cells have a significantly altered sphingolipid metabolism (*i.e.*, lower intrinsic ASM activity), which sensitizes cancer cells to the CAD-induced LMP.[39,88,90] As we show that nonlethal LMP is sufficient to considerably promote small NA delivery *in vitro*, we anticipate that CADs could reach target cancer cells in appropriate concentrations to enable their use as small NA delivery-enhancing compounds.[19,38] Of note, antidepressant CADs (*e.g.*, amitriptyline, fluoxetine) were also shown to decrease ASM activity *in vivo* in noncancerous tissues, such as the hippocampus (oral administration) or lungs (inhalation or intraperitoneal injection) of mice.[91−94] Likewise, the CAD-induced cellular phenotypes (*e.g.*,

https://dx.doi.org/10.1021/acsnano.0c00666
ACS Nano 2020, 14, 4774−4791

functional inhibition of ASM, PLD induction, lysosomal swelling) have also been described in endothelial cells and macrophages, which are generally the first cells encountered by nanocarriers upon systemic administration.[95−100] Altogether, these data indicate that the concept of CAD repurposing to promote small NA delivery could be practicable *in vivo*, as well. Nonetheless, as CADs and NPs need to be present in the same intracellular compartment to enable the adjuvant effect, coencapsulation of the CAD and the small NA in the same NP and/or local application (*e.g.*, topical, pulmonary) should improve control over extra- and intracellular distribution, thus contributing to a successful *in vivo* translation.[14,101]

CONCLUSION

The data presented here clearly demonstrate that multiple CADs can be repurposed as potent adjuvants to promote cytosolic siRNA and ASO delivery in distinct cell lines. As inefficient cellular delivery to date remains the most important cellular barrier for NA therapeutics and many CADs are clinically approved drugs, this adjuvant strategy can be exploited as leverage for clinical translation. Moreover, as the identified NA delivery-promoting CADs have diverging pharmacological action, such a combination therapy can provide synergistic therapeutic effects. Importantly, our data also indicate that the CAD adjuvant approach is carrier-specific, likely providing benefit mainly for nanomedicines that entail a substantial endolysosomal pool of decomplexed NAs to diffuse through the CAD-induced pores in the limiting endolysosomal membrane.[19] In contrast to the governing nanomedicine model, stating that cytosolic release of siRNA should ideally occur prior to fusion of endosomes with the degradative lysosomes, these data support the rational design of nanocarriers that release their NA payload in the lysosomal lumen with the aim to maximize the CAD adjuvant effect.

MATERIALS AND METHODS

siRNA Duplexes and Oligonucleotides. The 21mer siRNA duplexes targeted against the enhanced green fluorescent protein (eGFP, sieGFP), pGL3 (luc+ gene), and pGL4 (luc2 gene) firefly luciferase (siLUC+ and siLUC2) and the negative control siRNA (siCTRL) were purchased from Eurogentec (Seraing, Belgium). The 16mer phosphorothioate gapmer antisense oligonucleotides (ASOs) with locked nucleic acid (LNA) modifications targeting eGFP (ASO-eGFP) were also purchased from Eurogentec (Seraing, Belgium).[102] A phosphorothioate negative control gapmer ASO with LNA modifications (antisense LNA gapmer control, negative control A, ASO-CTRL) was from Qiagen (Germantown, USA). Both negative controls (siRNA and ASO) consist of a sequence that has no relevant homology to any known eukaryotic gene sequences. Fluorescent siCTRL and ASO-eGFP were labeled with a Cy5 dye at the 5′ end of the (sense) strand (respectively, abbreviated siCy5 and ASO-Cy5 (Eurogentec, Seraing, Belgium)). AlexaFluor647-labeled 21mer oligonucleotides (AF647 ONs) were from Eurogentec (Seraing, Belgium), as well. The concentration of the siRNA/ASO/ON stock solutions in nuclease-free water (Ambion-Life Technologies, Ghent, Belgium) was calculated from absorption measurements at 260 nm (1 OD_{260} = 40 $\mu g\,mL^{-1}$) with a NanoDrop 2000c UV−vis spectrophotometer (Thermo Fisher Scientific, Rockford, IL, USA). The sequences and modifications of the applied siRNA duplexes/ASOs/ONs are summarized in Table S2.

Nanoparticle Synthesis, Preparation, and siRNA Complexation. Dextran hydroxyethyl methacrylate or dextran methacrylate (dex-HEMA or dex-MA) was copolymerized with a cationic methacrylate monomer [2-(methacryloyloxy)ethyl]-trimethylammonium chloride (TMAEMA) to produce cationic dex-HEMA-*co*-TMAEMA (degree of substitution (DS) of 5.2) and dex-MA-*co*-TMAEMA (DS of 5.9) nanogels (hereafter abbreviated as respectively dex-HEMA NGs and dex-MA NGs), using an inverse miniemulsion photopolymerization method as reported previously.[9,25,26,28,30] To ensure long-term stability, the NGs were lyophilized and stored desiccated. Propylamine-functionalized MSNPs (particle size of 200 nm as documented by manufacturer, pore size = 4 nm) were obtained from Sigma-Aldrich (Overijse, Belgium). To obtain ASO/siRNA-loaded NGs or MSNPs (ASO-/siNGs or siMSNPs) for *in vitro* experiments, a stock (2 mg/mL) was prepared by dispersing a weighed amount of particles in ice-cooled nuclease-free water (Ambion-Life Technologies, Ghent, Belgium), followed by sonication (3 × 5 s, amplitude 10% for NGs; 1 × 3 min, amplitude 15%, 10 s on/10 s off for MSNPs; Branson Digital Sonifier, Danbury, CT, USA). Subsequently, equal volumes of NG/MSNP and siRNA/ASO dilutions in 4-(2-hydroxyethyl)-1-piperazineethanesulfonic acid (HEPES) buffer (pH 7.4, 20 mM) were mixed and incubated at 4 °C for 10 min to allow electrostatic complexation, prior to further dilution in Opti-MEM (Invitrogen, Merelbeke, Belgium). This complexation procedure was applied for all cell-based experiments in a 96-well plate and resulted in a 30 μg/mL NG dispersion loaded with 1 nM siRNA (0.033 pmol siRNA/μg NGs or 0.1 pmol siRNA/well) or 100−250 nM ASO (3.3−8.3 pmol ASO/μg NGs or 10−25 pmol ASO/well) for the H1299-eGFP cells, unless indicated otherwise. In 24-well plates (Figure S1A,B) or 35 mm diameter CELLview microscopy dishes with a glass bottom (Greiner Bio-One GmbH, Vilvoorde, Belgium), a NG dispersion of 30 μg/mL loaded with 2 nM siRNA (0.067 pmol siRNA/μg NGs or 0.6 pmol siRNA/well or 1.8 pmol siRNA/dish) was applied, unless indicated otherwise. SKOV-3-LUC+, SKOV-3-LUC2 IP2, and HeLa NLS-GFP cells were transfected in 96-well plates with a 25 μg/mL NG dispersion loaded with, respectively, 2 and 10 nM (the latter two) siRNA (0.080 and 0.4 pmol siRNA/μg NGs or 0.2 and 1 pmol siRNA/well), unless indicated otherwise. In the case of the siMSNPs, a dispersion of 30 μg/mL loaded with 10 or 20 nM siRNA (0.334−0.667 pmol siRNA/μg MSNP or 1−2 pmol siRNA/well) was applied in 96-well plates.

Lipofectamine RNAiMAX (LF RNAiMAX) (Thermo Fisher Scientific, Rockford, USA) was applied as prescribed by the manufacturer. In short, equal volumes of LF RNAiMAX and siRNA dilutions in Opti-MEM were mixed and allowed to complex during 5 min at room temperature. The subsequent cell transfection occurred in Opti-MEM for 4 h at 37 °C. According to the guidelines, 1 pmol siRNA/well (10 nM siRNA) and 0.25 μL of LF RNAiMAX/well were applied to obtain optimal transfection efficiencies in 96-well plates. Additionally, the LF RNAiMAX lipoplexes were further diluted to 0.5, 0.1, 0.05, and 0.025 pmol siRNA/well.

DOTAP ((2,3-dioleoyloxypropyl)trimethylammonium)−DOPE (1,2-dioleoyl-*sn*-glycero-3-phosphoethanolamine) LIPs were prepared *via* the lipid film hydration method. All lipids were obtained from Avanti Polar Lipids, Inc. (Alabaster, AL, USA) as solutions in chloroform. Appropriate volumes of the lipid solutions were mixed in a round-bottom flask to obtain a 1:1 molar ratio. For the preparation of PEGylated LIP, the desired amounts of DSPE-PEG_{2000} (1,2-distearoyl-*sn*-glycero-3-phosphoethanolamine-*N*-[methoxy(polyethylene glycol)-2000]) dissolved in chloroform (corresponding to 5 mol % of the total lipids) were added to the lipids in the round-bottomed flask. Through rotary evaporation under vacuum at 40 °C, a lipid film was created and subsequently hydrated using 1 mL of HEPES buffer (pH 7.4, 20 mM). The obtained mixture was vortexed and sonicated for 1 min at 10% amplitude to obtain a monodisperse 2 mM LIP dispersion (total lipid concentration). Hydrodynamic diameter and zeta-potential of these (PEGylated) DOTAP-DOPE LIP were determined *via* dynamic light scattering (DLS, Figure S10A) (Zetasizer Nano, Malvern Instruments, Worcestershire, United Kingdom). Subsequently, siRNA was complexed with the (PEGylated) DOTAP-DOPE LIP at an optimal charge ratio equal to eight.[76] Hereto, equal volumes of LIP and siRNA in HEPES buffer were mixed and allowed to complex at room temperature for 30 min prior to further dilution in Opti-MEM and transfection.

Preparation of lipid nanoparticles, containing the ionizable lipid MC3 (MC3 siLNPs), is described in Supporting Information.

Fluorescence Fluctuation Spectroscopy on siRNA-Loaded NPs. Fluorescence fluctuation spectroscopy is a microscopy-based

https://dx.doi.org/10.1021/acsnano.0c00666
ACS Nano 2020, 14, 4774−4791

technique that monitors the fluorescence intensity fluctuations of fluorescent molecules diffusing in and out of the focal volume (a fixed excitation volume) of a confocal microscope.[25,30,77] Previous work by our group used FFS to quantify the complexation of fluorescently labeled siRNA to various nanocarriers.[9,25,30,73,76,77] In this study, FFS experiments were carried out on dex-HEMA NGs, (PEGylated) DOTAP-DOPE LIP and MSNPs, loaded with siCy5 (0.033 pmol siRNA/μg NGs, 0.667 pmol siRNA/μg MSNP and a charge ratio of 8 for the (PEGylated) DOTAP-DOPE LIP). Next, the release of siRNA from the NPs was evaluated in the presence of competing polyanions (10 kDa dextran sulfate sodium salt, Sigma-Aldrich). Equal volumes of DEXS and siRNA-loaded NPs in HEPES buffer were mixed, resulting in a final siRNA concentration of 25 nM. After 10 min incubation at room temperature, the samples were transferred to a glass-bottom 96-well plate (Greiner Bio-One GmbH, Frickenhausen, Germany) and the focal volume of the microscope was positioned in the sample, followed by the recording of the fluorescence fluctuations during a 60 s time interval. Samples were measured in triplicate for three independent experiments. The average fluorescence intensity of freely diffusing and complexed siRNA in the fluorescence fluctuation profile was determined as described previously.[25,30,77] FFS measurements were performed with a laser scanning confocal microscope (C2si, Nikon, Japan) equipped with a water immersion objective lens (Plan Apo 60×, NA 1.2, collar rim correction, Nikon, NY, USA), using a 633 nm laser line for the excitation of fluorescent siRNA (siCy5). Fluorescence was detected with the detection channels of the fluorescence correlation spectrometer MicroTime 200 (Picoquant GmbH, Berlin, Germany) that was equipped with SymPhoTime software (Picoquant GmbH, Germany).

Cell Lines and Cell Culture Conditions. The human non-small cell lung epithelial carcinoma cell line (H1299) that stably expresses eGFP (H1299-eGFP), the human ovarian cancer cell line (SKOV-3) that stably expresses the pGL3 firefly luciferase (SKOV-3-LUC+), the *in vivo* selected SKOV-3 IP2 cell line that stably expresses the pGL4 firefly luciferase (SKOV-3-LUC2 IP2), and the HeLa cells stably transfected with a nuclear-localized signaling expressing GFP (HeLa NLS-GFP) were, respectively, obtained from the lab of Prof. Camilla Foged (Department of Pharmacy, University of Copenhagen, Denmark), the lab of Prof. Achim Aigner (Institute of Pharmacology, Pharmacy and Toxicology, University of Leipzig, Germany), the lab of Prof. Olivier De Wever (Laboratory of Experimental Cancer Research, Ghent University, Belgium), and the lab of Prof. Winnok H. De Vos (Laboratory of Cell Biology and Histology, University of Antwerp, Belgium).[19,28,103−108] The wild-type variant of the H1299 cells (H1299-WT, ATCC CRL-5803) was obtained from American Type Culture Collection (ATCC, Manassas, VA, USA). H1299 cells (H1299-WT and H1299-eGFP), SKOV-3 cells, and HeLa NLS-GFP cells were, respectively, maintained in Roswell Park Memorial Institute (RPMI) 1640 culture medium, McCoy's 5A culture medium, and Dulbecco's modified Eagle medium (supplemented with growth factor F12; DMEM/F-12) culture medium, all supplemented with 10% fetal bovine serum (FBS, Hyclone, GE Healthcare, Machelen, Belgium), 2 mM L-Glutamine and 100 U/mL penicillin/streptomycin (hereafter collectively called "complete cell culture medium" or CCM). The cell lines were cultured in a humidified atmosphere containing 5% CO_2 at 37 °C and culture medium was renewed every other day unless the 80% confluence level was reached. In this case, the cells were split using 0.25% trypsin-ethylenediaminetetraacetic acid (EDTA). For eGFP transgene selection, H1299-eGFP cells were treated with medium containing 1 mg/mL Geneticin once per month. All cells were regularly tested and found negative for mycoplasma. All products were purchased from Gibco-Life Technologies (Grand Island, NY, USA) unless specifically mentioned otherwise.

Compound Library Stock Preparation and Small Molecules. The NIHCC library was acquired from Evotec (San Francisco, CA, USA), which supplied the DMSO-dissolved compounds at a concentration of 10 mM. Stock plates were made by transferring 2 μL of each compound to a new 96-well plate, followed by dilution to 10 μL with sterile-filtered BioPerformance Certified dimethyl sulfoxide (DMSO, Sigma-Aldrich, Overijse, Belgium), resulting in a concentration of 2 mM for each compound. Two microliters of the latter stock solutions was diluted with 198 μL of serum-containing complete cell culture medium (CCM) directly before use to give a final concentration of 20 μM for each drug. The final DMSO concentration brought onto the cells (both compound-treated and DMSO control) was 1% (v/v). Note that apart from the NIHCC-compounds, all the small molecules were obtained from Sigma-Aldrich (Overijse, Belgium), except loperamide HCl (LKT Laboratories Inc., St. Paul, MN, USA), and the stock solutions were also prepared in sterile-filtered BioPerformance Certified dimethyl sulfoxide (DMSO, Sigma-Aldrich, Overijse, Belgium).

NIHCC Screening Protocol. H1299-eGFP cells were seeded in 96-well plates (SPL Lifesciences Co. Ltd., Naechon-Myeon Pocheon, South Korea) at a density of 7500 cells/well (100 μL/well) and were allowed to settle overnight. Next, the cells were transfected with dex-HEMA siNGs (0.1 pmol siRNA/well, prepared as described above) during 4 h at 37 °C in a humidified atmosphere containing 5% CO_2. Note that for every sieGFP condition a siCTRL sample was included to account for potential off-target effects. Subsequently, the siNG dispersion was removed and the cells received 50 μL fresh (DMSO control) or compound-containing CCM (20 μM). Each 96-well plate contained a siNG-DMSO control (n = 4, 4 siCTRL and 4 sieGFP conditions) and 50 wells treated with 25 compounds (20 μM, n = 1, 1 siCTRL and 1 sieGFP condition). After 20 h, the small molecule containing CCM (and DMSO control) was removed and cells were kept in 50 μL fresh CCM for an additional 24 h until flow cytometry analysis. Sample preparation consisted of detachment with 30 μL 0.25% trypsin-EDTA, neutralization with 120 μL CCM and a transfer of the cell suspensions to a U-bottom 96-well plate (Greiner Bio-One GmbH, Vilvoorde, Belgium), which was centrifuged during 5 min at 500 g. After removal of 120 μL supernatant, the cells were resuspended in 80 μL flow buffer (phosphate buffered saline (PBS, no calcium, no magnesium) with 1% (v/v) FBS (Hyclone, GE Healthcare, Machelen, Belgium) and 0.1% (w/v) sodium azide (Sigma-Aldrich, Overijse, Belgium)) and kept on ice until analysis. For each sample the forward and side scatter (respectively FSC and SSC) as well as the green fluorescent signal of single cells were measured for 100 s at a flow rate of 25 μL/min. The samples were excited with the 488 nm laser line and the signal was detected with the 530/30 filter using the Attune NxT flow cytometer with the Attune auto sampler (Applied Biosystems by Life Technologies, Foster City, CA, USA) and Attune NxT acquisition software. Finally, data analysis was performed using the FlowJo software (Tree Star Inc., Ashland, OR, USA) and data were exported into Microsoft Excel (16th version, Microsoft Corp., Redmond, WA, USA) for hit classification. The detailed hit identification procedure is provided in the Supporting Information.

Quantification of Transfection Efficiency/Lysosomal Volume of NP Transfection and Sequential Adjuvant Treatment by Flow Cytometry. Other transfection experiments with H1299-eGFP cells were performed similar to the above-mentioned screening protocol. Following 20 h of CAD treatment (KET, LOP, DES) with the indicated concentrations (maximally 0.08% (v/v) residual DMSO), the lysosomes were labeled with the LysoTracker Deep Red (LDR) probe (Molecular Probes, Eugene, OR, USA) through incubation with 50 μL 75 nM LDR in CCM for 30 min at 37 °C. After removal of the LDR-containing CCM and a washing step with 30 μL PBS, further sample preparations were carried out as described above. For each sample the FSC and SSC as well as the green and red fluorescent signal of single cells were measured. The samples were excited with the 488 and 638 nm laser lines and the signal was detected with the 525/40 and 660/20 filters using the CytoFLEX flow cytometer with plate loader for 96-well plates (Beckman Coulter, Krefeld, Germany) and CytExpert software. FlowJo software was used for data analysis as described above. The calculated percentages eGFP expression and fold changes in LDR signal intensity/SSC signal are presented as the mean ± standard error of the mean for minimum 3 independent repeats (biological replicates), unless otherwise indicated. In an additional experiment (Figure S1A-B), H1299-eGFP cells (seeded at 35000 cells/well) were transfected in 24-well plates with dex-HEMA siNGs for 4 h at 37 °C as described before.[19] Note that in this experiment the indicated DES concen-

https://dx.doi.org/10.1021/acsnano.0c00666
ACS Nano 2020, 14, 4774−4791

trations (applied in preincubation (Pre), immediately after (Post) or 20 h after transfection (20 h Post)) were only applied on the cells for 2 h. LysoTracker Deep Red (LDR) staining was performed similar to the aforementioned protocol. Transfection procedure and transfection efficiency determination of SKOV-3-LUC+/2 (IP2) and HeLa NLS-GFP cells is detailed described in Supporting Information.

Cell Viability. H1299-eGFP cells were seeded, transfected with dex-HEMA siNGs and treated with the CADs similar to the silencing experiments. The cell viability was determined with the CellTiter GLO assay (Promega, Belgium). According to manufacturer instructions, the culture plates and reconstituted assay buffer were placed at room temperature for 30 min, before initiating the assay. Subsequently, the CCM was replaced by 100 μL fresh CCM and an equal amount of assay buffer was added. To induce complete cell lysis, the plates were shaken during 2 min and the signal was allowed to stabilize the following 10 min. Next, 100 μL from each well was transferred to an opaque 96-well plate, which was measured with a GloMax 96 Microplate Luminometer (Promega, Belgium). Data are presented as the mean cell viability (%, percentage of luminescent signal relative to nontreated cells (NTC) for each condition) ± standard error of the mean for minimum three independent repeats.

Quantification of *In Vitro* Cellular ASO or siRNA Internalization in H1299-eGFP and SKOV-3-LUC+ Cells by Flow Cytometry. To quantify the cellular uptake of ASO or siRNA by flow cytometry, H1299-eGFP and SKOV-3-LUC+ cells were seeded in 96-well plates at a density of 7500 cells/well and left to settle overnight. NPs were loaded with different amounts of siCTRL:siCy5 or ASO-CTRL:ASO-Cy5 (90:10 mol %). Following dilution in Opti-MEM (final NP concentrations are described above), the particles were incubated with the cells for 3 h (SKOV-3-LUC+ cells) or 4 h (H1299-eGFP) (37 °C, 5% CO_2). Next, the cells were washed with dextran sulfate sodium salt (1 mg/mL in PBS) to remove cell surface-bound fluorescence. Further sample preparations were carried out as previously described for the silencing experiments.

Visualizing eGFP Expression with Confocal Microscopy. H1299-eGFP cells were seeded at 105000 cells/dish in 35 mm diameter CELLview microscopy dishes with glass bottom (Greiner Bio-One GmbH, Vilvoorde, Belgium) and were allowed to settle overnight. After removal of the complete CCM, the cells were transfected with 900 μL of a 30 μg/mL NG dispersion loaded with 2 nM siRNA (=0.067 pmol siRNA/μg NGs or 1.8 pmol siRNA/dish). Following incubation for 4 h (37 °C, 5% CO_2), the siNG dispersion was removed and the cells were washed once with phosphate buffered saline (PBS, Invitrogen, Merelbeke, Belgium). Next, the cells received 1.5 mL of fresh CCM, containing different micromolar concentrations of LOP/KET or a DMSO control for 20 h (37 °C, 5% CO_2). Subsequently, the CAD-containing CCM was removed and cells were kept in 1.5 mL of fresh CCM for an additional 24 h. Before confocal imaging, the cells were fixed with 4% paraformaldehyde during 15 min at room temperature. After a double washing step with PBS, the cells were finally stored at 4 °C until imaged in Vectashield antifade mounting medium containing DAPI (Vector Laboratories, Burlingame, VT, USA). A spinning disk confocal (SDC) microscope (Nikon Eclipse Ti, Japan), equipped with a MLC 400 B laser box (Agilent Technologies, USA), a Yokogawa CSU-X confocal spinning disk device (Andor, Belfast, UK), an iXon ultra EMCCD camera (Andor Technology, Belfast, UK), a Plan Apo VC 60× 1.4 NA oil immersion objective lens (Nikon, Japan) and NIS Elements software (Nikon, Japan) was applied for imaging. The 408 and 488 nm laser lines were, respectively, used to excite the DAPI-labeled nuclei and the eGFP protein. A wait command of 0.2 s between the image acquisition of the two channels was applied to avoid spectral overlap of the DAPI dye and the eGFP protein.

Visualization and Quantification of the Cytosolic Release of siCy5 and AF647 ONs. H1299-WT cells (siCy5 release experiment), H1299-eGFP (AF647 ONs release experiment), and SKOV-3-LUC2 IP2 cells (AF647 ONs release experiment) were seeded at, respectively, 105000 (H1299-WT) and 200000 (H1299-eGFP, SKOV-3-LUC2 IP2) cells/dish in 35 mm diameter glass-bottom microscopy dishes (Greiner Bio-One GmbH, Germany) and were allowed to settle overnight. To visualize the siCy5 release, dex-HEMA NGs were first loaded with 100 nM siCy5 and subsequently added to each dish as described above (3.35 pmol siCy5/μg NGs, 4 h incubation). To assess AF647 ON escape, the dex-HEMA NGs were likewise loaded with 25 nM AF647 ONs and subsequently added to each dish as described above (0.833 pmol AF647 ONs/μg NGs, 4 h incubation for H1299-eGFP cells and 1 pmol AF647 ONs/μg NGs, 3 h incubation for SKOV-3-LUC2 IP2 cells). Further steps (*e.g.*, CAD treatments, imaging) were done as described above for visualizing the eGFP expression with confocal microscopy, unless mentioned otherwise. No fixation step was applied, but an extra washing step with dextran sulfate sodium salt (1 mg/mL in PBS) was done after removal of the dex-HEMA si-/ON-NG dispersion. After removal of the small-molecule-containing CCM, the nuclei were labeled with Hoechst 33342 (Molecular Probes, Belgium) in CCM (1 mg/mL in water, 1/1000 dilution) during 15 min at 37 °C. Finally, the Hoechst solution was removed, fresh CCM was added, and cells were kept at 37 °C in a humidified atmosphere containing 5% CO_2 until imaging. The 408 and 633 nm laser lines were applied to excite the Hoechst-labeled nuclei and the fluorescence resulting from the siCy5 and AF647 ONs, respectively. To detect the faint cytosolic staining of siCy5, a long exposure time of 500 ms was used for the red channel as described before.[8] In the case of the AF647 ONs, if endolysosomal escape occurs, the labeled ONs will spread toward the cytosol, dequench, and finally accumulate into the nucleus.[109,110] During data analysis with ImageJ (FIJI) software, both the total cell number and amount of cells with a diffuse siCy5 labeling or AF647 ON-positive nuclei were counted. In the AF647 ON experiments, nuclei were detected in the blue channel by thresholding (applying the same offset values for every image), and intensity analysis (mean gray value) of the nuclear fluorescence signal in the red channel was done. Using the sixth version of the GraphPad Prism software, these intensity values were plotted in frequency distributions and, based on these histograms, a percentage of cells with AF647 ON-positive nuclei was determined. Data are represented as the percentage of cells with a diffuse siCy5 signal for minimum 278 cells per condition in minimum 42 images and the percentage of cells with AF647 ON-positive nuclei for at least 545 cells in minimum 53 images.

Phospholipidosis Detection with LipidTOX Red. H1299-eGFP cells were seeded (200000 cells/dish) and allowed to settle overnight as specified for the AF647 ON release experiment. Next, the cells were incubated with a mixture of a 1/1000 dilution of the LipidTOX Red phospholipidosis detection reagent (Thermo Fisher Scientific, Rockford, USA) and the desired CAD in CCM. Upon 20 h incubation, the nuclei were labeled with Hoechst 33342 (Molecular Probes, Belgium) as detailed for the AF647 ON release experiment. The 408 and 561 nm laser lines were applied to excite the Hoechst-labeled nuclei and the fluorescence resulting from the LipidTOX Red phospholipidosis dye, respectively. Imaging occurred with a Plan Apo VC 100× 1.4 NA oil immersion objective lens (Nikon, Japan) and a SDC microscope as described above for visualizing the eGFP expression with confocal microscopy. The LipidTOX Red phospholipidosis signal area was determined with ImageJ (FIJI) in at least 432 cells from 62 images. To this end, all confocal images were processed by applying the same offset values for the LipidTOX Red phospholipidosis signal. In each image, both the number of cells and signal area of the LipidTOX Red phospholipidosis dye was determined to allow calculation of the normalized LipidTOX Red phospholipidosis area (*i.e.*, LipidTOX Red phospholipidosis signal area/cell number) in each image. The fold change in LipidTOX Red phospholipidosis signal area was calculated by dividing the normalized signal area in treated cells by the normalized signal area in untreated cells.

Statistical Analysis. Statistical analysis was performed using the sixth version of the GraphPad Prism software. One-way ANOVA combined with the posthoc Dunnett test was applied to compare multiple conditions, whereas the student *t*-test was used for direct comparison of 2 conditions. χ^2 likelihood ratio tests with Yates continuity correction were used to analyze 2 × 2 contingency tables to check statistical dependence of the two properties shown in the contingency tables. Multiple linear regression analysis was performed with normalized eGFP expression as a dependent variable. A p value ≤ 0.05 was considered *a priori* to be statistically significant.

https://dx.doi.org/10.1021/acsnano.0c00666
ACS Nano 2020, 14, 4774−4791

ASSOCIATED CONTENT

Supporting Information

The Supporting Information is available free of charge at https://pubs.acs.org/doi/10.1021/acsnano.0c00666.

Preincubation of DES in H1299-eGFP cells; hit selection procedure, association of screened compounds ("hits" and "no hits") with published drug characteristics and PCA analysis; hit adjuvant compounds that comply with the CAD definition; fold change in SSC signal for LOP and KET treatment in H1299-eGFP cells; fold change in LipidTOX signal area, cell viability, and BODIPY FL C 12-SM signal for multiple CADs in H1299-eGFP cells; CADs increase small NA release to the cytosol, leading to an enhanced dex-HEMA siNG LUC/GFP silencing potential in SKOV-3-LUC and HeLa NLS-GFP cells; schematic representation of the tested siNPs; effect of sequential DES treatment on LDR signal in combination with (PEGylated) DOTAP-DOPE siLIP in H1299-eGFP cells; effect of sequential DES treatment on the silencing potential of siRNA-loaded RNAiMAX LIP and the LDR signal in H1299-eGFP cells; physicochemical properties of the (PEGylated) DOTAP-DOPE LIP and the visual representation of lipoplex formation; physicochemical properties of MC3 siLNPs; effect of sequential DES treatment on the silencing potential of MC3 siLNPs and the LDR signal in H1299-eGFP cells; decomplexation efficiency and uptake of MC3 siLNPs; CADs improve cytosolic release of FITC-dextrans up to 150 kDa in H1299-WT cells; applied siRNA/ASO/ON sequences and modifications; hit identification procedure, the quantification of siNG transfection efficiency in SKOV-3-LUC and HeLa NLS-GFP cells, MC3 siLNPs (synthesis, DLS, transfection, uptake, agarose gel electrophoresis, Quant-iT RiboGreen RNA assay), visualization of the cytosolic release of FITC-dextrans, BODIPY FL C12-sphingomyelin staining (PDF)

AUTHOR INFORMATION

Corresponding Author

Koen Raemdonck − *Ghent Research Group on Nanomedicines, Laboratory of General Biochemistry and Physical Pharmacy, Faculty of Pharmaceutical Sciences, Ghent University, 9000 Ghent, Belgium*; Phone: +32 9 264 80 78; Email: Koen.Raemdonck@UGent.be; Fax: +32 9 264 81 89

Authors

Thijs Van de Vyver − *Ghent Research Group on Nanomedicines, Laboratory of General Biochemistry and Physical Pharmacy, Faculty of Pharmaceutical Sciences, Ghent University, 9000 Ghent, Belgium*; orcid.org/0000-0002-8030-6768

Bram Bogaert − *Ghent Research Group on Nanomedicines, Laboratory of General Biochemistry and Physical Pharmacy, Faculty of Pharmaceutical Sciences, Ghent University, 9000 Ghent, Belgium*

Lynn De Backer − *Ghent Research Group on Nanomedicines, Laboratory of General Biochemistry and Physical Pharmacy, Faculty of Pharmaceutical Sciences, Ghent University, 9000 Ghent, Belgium*

Freya Joris − *Ghent Research Group on Nanomedicines, Laboratory of General Biochemistry and Physical Pharmacy, Faculty of Pharmaceutical Sciences, Ghent University, 9000 Ghent, Belgium*

Roberta Guagliardo − *Ghent Research Group on Nanomedicines, Laboratory of General Biochemistry and Physical Pharmacy, Faculty of Pharmaceutical Sciences, Ghent University, 9000 Ghent, Belgium*

Jelter Van Hoeck − *Ghent Research Group on Nanomedicines, Laboratory of General Biochemistry and Physical Pharmacy, Faculty of Pharmaceutical Sciences, Ghent University, 9000 Ghent, Belgium*

Pieterjan Merckx − *Ghent Research Group on Nanomedicines, Laboratory of General Biochemistry and Physical Pharmacy, Faculty of Pharmaceutical Sciences, Ghent University, 9000 Ghent, Belgium*; orcid.org/0000-0002-3274-6144

Serge Van Calenbergh − *Laboratory for Medicinal Chemistry, Faculty of Pharmaceutical Sciences, Ghent University, 9000 Ghent, Belgium*; orcid.org/0000-0002-4201-1264

Srinivas Ramishetti − *Laboratory of Precision NanoMedicine, School of Molecular Cell Biology and Biotechnology, George S. Wise Faculty of Life Sciences, Department of Materials Sciences and Engineering, Iby and Aladar Fleischman Faculty of Engineering, and Center for Nanoscience and Nanotechnology, Cancer Biology Research Center, Tel Aviv University, Tel Aviv 6997801, Israel*

Dan Peer − *Laboratory of Precision NanoMedicine, School of Molecular Cell Biology and Biotechnology, George S. Wise Faculty of Life Sciences, Department of Materials Sciences and Engineering, Iby and Aladar Fleischman Faculty of Engineering, and Center for Nanoscience and Nanotechnology, Cancer Biology Research Center, Tel Aviv University, Tel Aviv 6997801, Israel*; orcid.org/0000-0001-8238-0673

Katrien Remaut − *Ghent Research Group on Nanomedicines, Laboratory of General Biochemistry and Physical Pharmacy, Faculty of Pharmaceutical Sciences, Ghent University, 9000 Ghent, Belgium*

Stefaan C. De Smedt − *Ghent Research Group on Nanomedicines, Laboratory of General Biochemistry and Physical Pharmacy, Faculty of Pharmaceutical Sciences, Ghent University, 9000 Ghent, Belgium*; orcid.org/0000-0002-8653-2598

Complete contact information is available at: https://pubs.acs.org/10.1021/acsnano.0c00666

Author Contributions

Conceptualization and study design: T.V.d.V, S.C.D.S., and K. Raemdonck. Experimental work and data analysis: T.V.d.V., B.B., L.D.B., R.G., P.M., F.J., J.V.H., K. Remaut, and K. Raemdonck. S.V.C. contributed to the compound screen. S.R. and D.P. assisted with the design and evaluation of the ionizable lipid nanoparticles. The manuscript was written through contributions of all authors. All authors have given approval to the final version of the manuscript.

Notes

The authors declare no competing financial interest.

ACKNOWLEDGMENTS

T.V.d.V. is a doctoral fellow of the Research Foundation-Flanders (Grant 1198719N, FWO, Belgium). B.B. is a doctoral fellow of the FWO (Grant 1S75019N). L.D.B. acknowledges the Special Research Fund of Ghent University (BOF12/GOA/014). F.J. acknowledges the Agency for Innovation by Science and Technology in Flanders (IWT, Belgium). R.G. is an early stage researcher within the NANOMED project, which has received funding from the European Union's Horizon 2020 Research and Innovation Programme Marie Skłodowska Curie

Innovative Training Networks (ITN) under Grant No. 676137. J.V.H. is a doctoral fellow of the FWO (Grant 1S62519N). P.M. is a doctoral fellow of the FWO (Grant 1S30618N). K. Raemdonck acknowledges the FWO for a postdoctoral Research Grant (Grant 1517516N). We thank Prof. T. Coenye and C. Rigauts from the Laboratory of Pharmaceutical Microbiology (UGent, Belgium) for the use of the Attune NxT flow cytometer. We also thank Prof. R. Vandenbroucke from the VIB-UGent Center for Inflammation Research (Ghent, Belgium) for the use of the microfluidic NanoAssemblr® Benchtop mixing device.

REFERENCES

(1) Dowdy, S. F. Overcoming Cellular Barriers for RNA Therapeutics. *Nat. Biotechnol.* **2017**, *35*, 222−229.
(2) Wittrup, A.; Lieberman, J. Knocking down Disease: A Progress Report on SiRNA Therapeutics. *Nat. Rev. Genet.* **2015**, *16*, 543−552.
(3) Shen, X.; Corey, D. R. Chemistry, Mechanism and Clinical Status of Antisense Oligonucleotides and Duplex RNAs. *Nucleic Acids Res.* **2018**, *46*, 1584−1600.
(4) Kanasty, R.; Dorkin, J. R.; Vegas, A.; Anderson, D. Delivery Materials for SiRNA Therapeutics. *Nat. Mater.* **2013**, *12*, 967−977.
(5) Yin, H.; Kanasty, R. L.; Eltoukhy, A. A.; Vegas, A. J.; Dorkin, J. R.; Anderson, D. G. Non-Viral Vectors for Gene-Based Therapy. *Nat. Rev. Genet.* **2014**, *15*, 541−555.
(6) Martens, T. F.; Remaut, K.; Demeester, J.; De Smedt, S. C.; Braeckmans, K. Intracellular Delivery of Nanomaterials: How to Catch Endosomal Escape in the Act. *Nano Today* **2014**, *9*, 344−364.
(7) Gilleron, J.; Querbes, W.; Zeigerer, A.; Borodovsky, A.; Marsico, G.; Schubert, U.; Manygoats, K.; Seifert, S.; Andree, C.; Stöter, M.; Epstein-Barash, H.; Zhang, L.; Koteliansky, V.; Fitzgerald, K.; Fava, E.; Bickle, M.; Kalaidzidis, Y.; Akinc, A.; Maier, M.; Zerial, M. Image-Based Analysis of Lipid Nanoparticle−Mediated SiRNA Delivery, Intracellular Trafficking and Endosomal Escape. *Nat. Biotechnol.* **2013**, *31*, 638−646.
(8) Wittrup, A.; Ai, A.; Liu, X.; Hamar, P.; Trifonova, R.; Charisse, K.; Manoharan, M.; Kirchhausen, T.; Lieberman, J. Visualizing Lipid-Formulated SiRNA Release from Endosomes and Target Gene Knockdown. *Nat. Biotechnol.* **2015**, *33*, 870−876.
(9) Raemdonck, K.; Naeye, B.; Buyens, K.; Vandenbroucke, R. E.; Høgset, A.; Demeester, J.; De Smedt, S. C. Biodegradable Dextran Nanogels for RNA Interference: Focusing on Endosomal Escape and Intracellular SiRNA Delivery. *Adv. Funct. Mater.* **2009**, *19*, 1406−1415.
(10) Sahay, G.; Querbes, W.; Alabi, C.; Eltoukhy, A.; Sarkar, S.; Zurenko, C.; Karagiannis, E.; Love, K.; Chen, D.; Zoncu, R.; Buganim, Y.; Schroeder, A.; Langer, R.; Anderson, D. G. Efficiency of SiRNA Delivery by Lipid Nanoparticles Is Limited by Endocytic Recycling. *Nat. Biotechnol.* **2013**, *31*, 653−658.
(11) Hirsch, M.; Helm, M. Live Cell Imaging of Duplex SiRNA Intracellular Trafficking. *Nucleic Acids Res.* **2015**, *43*, 4650−4660.
(12) Crooke, S. T.; Wang, S.; Vickers, T. A.; Shen, W.; Liang, X. Cellular Uptake and Trafficking of Antisense Oligonucleotides. *Nat. Biotechnol.* **2017**, *35*, 230−237.
(13) Ma, D. Enhancing Endosomal Escape for Nanoparticle Mediated SiRNA Delivery. *Nanoscale* **2014**, *6*, 6415−6425.
(14) Joris, F.; De Smedt, S. C.; Raemdonck, K. Small Molecules Convey Big Messages: Boosting Non-Viral Nucleic Acid Delivery with Low Molecular Weight Drugs. *Nano Today* **2017**, *16*, 14−29.
(15) Patel, S.; Ashwanikumar, N.; Robinson, E.; DuRoss, A.; Sun, C.; Murphy-Benenato, K. E.; Mihai, C.; Almarsson, Ö.; Sahay, G. Boosting Intracellular Delivery of Lipid Nanoparticle-Encapsulated MRNA. *Nano Lett.* **2017**, *17*, 5711−5718.
(16) Wang, L.; Ariyarathna, Y.; Ming, X.; Yang, B.; James, L. I.; Kreda, S. M.; Porter, M.; Janzen, W.; Juliano, R. L. A Novel Family of Small Molecules That Enhance the Intracellular Delivery and Pharmacological Effectiveness of Antisense and Splice Switching Oligonucleotides. *ACS Chem. Biol.* **2017**, *12*, 1999−2007.
(17) Juliano, R. L.; Wang, L.; Tavares, F.; Brown, E. G.; James, L.; Ariyarathna, Y.; Ming, X.; Mao, C.; Suto, M. Structure-Activity Relationships and Cellular Mechanism of Action of Small Molecules That Enhance the Delivery of Oligonucleotides. *Nucleic Acids Res.* **2018**, *46*, 1601−1613.
(18) Zhang, X.; Castanotto, D.; Liu, X.; Shemi, A.; Stein, C. A. Ammonium and Arsenic Trioxide Are Potent Facilitators of Oligonucleotide Function When Delivered by Gymnosis. *Nucleic Acids Res.* **2018**, *46*, 3612−3624.
(19) Joris, F.; De Backer, L.; Van de Vyver, T.; Bastiancich, C.; De Smedt, S. C.; Raemdonck, K. Repurposing Cationic Amphiphilic Drugs as Adjuvants to Induce Lysosomal SiRNA Escape in Nanogel Transfected Cells. *J. Controlled Release* **2018**, *269*, 266−276.
(20) Castanotto, D.; Zhang, X.; Alluin, J.; Zhang, X.; Rüger, J.; Armstrong, B.; Rossi, J.; Riggs, A.; Stein, C. A. A Stress-Induced Response Complex (SIRC) Shuttles MiRNAs, SiRNAs, and Oligonucleotides to the Nucleus. *Proc. Natl. Acad. Sci. U. S. A.* **2018**, *115*, E5756−E5765.
(21) Zhou, X.; Liu, Z.; Wang, H.; Liu, X.; Zhou, Z.; Tang, J.; Liu, X.; Zheng, M.; Shen, Y. SAHA (Vorinostat) Facilitates Functional Polymer-Based Gene Transfection *via* Upregulation of ROS and Synergizes with TRAIL Gene Delivery for Cancer Therapy. *J. Drug Target.* **2019**, *27*, 306−314.
(22) Gilleron, J.; Paramasivam, P.; Zeigerer, A.; Querbes, W.; Marsico, G.; Andree, C.; Seifert, S.; Amaya, P.; Stöter, M.; Koteliansky, V.; Waldmann, H.; Fitzgerald, K.; Kalaidzidis, Y.; Akinc, A.; Maier, M. A.; Manoharan, M.; Bickle, M.; Zerial, M. Identification of SiRNA Delivery Enhancers by a Chemical Library Screen. *Nucleic Acids Res.* **2015**, *43*, 7984−8001.
(23) Osborn, M. F.; Alterman, J. F.; Nikan, M.; Cao, H.; Didiot, M. C.; Hassler, M. R.; Coles, A. H.; Khvorova, A. Guanabenz (Wytensin™) Selectively Enhances Uptake and Efficacy of Hydrophobically Modified SiRNAs. *Nucleic Acids Res.* **2015**, *43*, 8664−8672.
(24) Yang, B.; Ming, X.; Cao, C.; Laing, B.; Yuan, A.; Porter, M. A.; Hull-Ryde, E. A.; Maddry, J.; Suto, M.; Janzen, W. P.; Juliano, R. L. High-Throughput Screening Identifies Small Molecules That Enhance the Pharmacological Effects of Oligonucleotides. *Nucleic Acids Res.* **2015**, *43*, 1987−1996.
(25) De Backer, L.; Braeckmans, K.; Demeester, J.; De Smedt, S. C.; Raemdonck, K. The Influence of Natural Pulmonary Surfactant on the Efficacy of SiRNA-Loaded Dextran Nanogels. *Nanomedicine* **2013**, *8*, 1625−1638.
(26) Raemdonck, K.; Naeye, B.; Høgset, A.; Demeester, J.; De Smedt, S. C. Prolonged Gene Silencing by Combining SiRNA Nanogels and Photochemical Internalization. *J. Controlled Release* **2010**, *145*, 281−288.
(27) Naeye, B.; Raemdonck, K.; Remaut, K.; Sproat, B.; Demeester, J.; De Smedt, S. C. PEGylation of Biodegradable Dextran Nanogels for SiRNA Delivery. *Eur. J. Pharm. Sci.* **2010**, *40*, 342−351.
(28) Merckx, P.; De Backer, L.; Van Hoecke, L.; Guagliardo, R.; Echaide, M.; Baatsen, P.; Olmeda, B.; Saelens, X.; Pérez-Gil, J.; De Smedt, S. C.; Raemdonck, K. Surfactant Protein B (SP-B) Enhances the Cellular SiRNA Delivery of Proteolipid Coated Nanogels for Inhalation Therapy. *Acta Biomater.* **2018**, *78*, 236−246.
(29) Jayaraman, M.; Ansell, S. M.; Mui, B. L.; Tam, Y. K.; Chen, J.; Du, X.; Butler, D.; Eltepu, L.; Matsuda, S.; Narayanannair, J. K.; Rajeev, K. G.; Hafez, I. M.; Akinc, A.; Maier, M. A.; Tracy, M. A.; Cullis, P. R.; Madden, T. D.; Manoharan, M.; Hope, M. J. Maximizing the Potency of SiRNA Lipid Nanoparticles for Hepatic Gene Silencing *In Vivo*. *Angew. Chem., Int. Ed.* **2012**, *51*, 8529−8533.
(30) De Backer, L.; Braeckmans, K.; Stuart, M. C. A.; Demeester, J.; De Smedt, S. C.; Raemdonck, K. Bio-Inspired Pulmonary Surfactant-Modified Nanogels: A Promising SiRNA Delivery System. *J. Controlled Release* **2015**, *206*, 177−186.
(31) Kornhuber, J.; Muehlbacher, M.; Trapp, S.; Pechmann, S.; Friedl, A.; Reichel, M.; Mühle, C.; Terfloth, L.; Groemer, T. W.; Spitzer, G. M.; Liedl, K. R.; Gulbins, E.; Tripal, P. Identification of Novel Functional Inhibitors of Acid Sphingomyelinase. *PLoS One* **2011**, *6*, No. e23852.
(32) Lepri, S.; Valeri, A.; Buratta, S.; Ceccarelli, M.; Bartolini, D.; Ruzziconi, R.; Goracci, L. Synthesis and Phospholipidosis Effect of a

https://dx.doi.org/10.1021/acsnano.0c00666
ACS Nano 2020, 14, 4774−4791

Series of Cationic Amphiphilic Compounds: A Case Study to Evaluate *In Silico* and *In Vitro* Assays. *Med. Chem. Res.* **2018**, *27*, 679−692.
(33) Devlin, J. P. Assay Technologies and Detection Methods. In *High Throughput Screening: The Discovery of Bioactive Substances*; Devlin, J. P., Ed.; Marcel Dekker: New York, 1997; pp 273−328.
(34) Muehlbacher, M.; Tripal, P.; Roas, F.; Kornhuber, J. Identification of Drugs Inducing Phospholipidosis by Novel *In Vitro* Data. *ChemMedChem* **2012**, *7*, 1925−1934.
(35) Goracci, L.; Ceccarelli, M.; Bonelli, D.; Cruciani, G. Modeling Phospholipidosis Induction: Reliability and Warnings. *J. Chem. Inf. Model.* **2013**, *53*, 1436−1446.
(36) Lemieux, B.; Percival, M. D.; Falgueyret, J.-P. Quantitation of the Lysosomotropic Character of Cationic Amphiphilic Drugs Using the Fluorescent Basic Amine Red DND-99. *Anal. Biochem.* **2004**, *327*, 247−251.
(37) Ishizaki, J.; Yokogawa, K.; Ichimura, F.; Ohkuma, S. Uptake of Imipramine in Rat Liver Lysosomes *In Vitro* and Its Inhibition by Basic Drugs. *J. Pharmacol. Exp. Ther.* **2000**, *294*, 1088−1098.
(38) Ellegaard, A.-M.; Dehlendorff, C.; Vind, A. C.; Anand, A.; Cederkvist, L.; Petersen, N. H. T.; Nylandsted, J.; Stenvang, J.; Mellemgaard, A.; Østerlind, K.; Friis, S.; Jäättelä, M. Repurposing Cationic Amphiphilic Antihistamines for Cancer Treatment. *EBioMedicine* **2016**, *9*, 130−139.
(39) Petersen, N. H. T.; Olsen, O. D.; Groth-Pedersen, L.; Ellegaard, A.-M.; Bilgin, M.; Redmer, S.; Ostenfeld, M. S.; Ulanet, D.; Dovmark, T. H.; Lønborg, A.; Vindeløv, S. D.; Hanahan, D.; Arenz, C.; Ejsing, C. S.; Kirkegaard, T.; Rohde, M.; Nylandsted, J.; Jäättelä, M. Transformation-Associated Changes in Sphingolipid Metabolism Sensitize Cells to Lysosomal Cell Death Induced by Inhibitors of Acid Sphingomyelinase. *Cancer Cell* **2013**, *24*, 379−393.
(40) Shahane, S. A.; Huang, R.; Gerhold, D.; Baxa, U.; Austin, C. P.; Xia, M. Detection of Phospholipidosis Induction: A Cell-Based Assay in High-Throughput and High-Content Format. *J. Biomol. Screening* **2014**, *19*, 66−76.
(41) Kornhuber, J.; Tripal, P.; Reichel, M.; Terfloth, L.; Bleich, S.; Wiltfang, J.; Gulbins, E. Identification of New Functional Inhibitors of Acid Sphingomyelinase Using a Structure-Property-Activity Relation Model. *J. Med. Chem.* **2008**, *51*, 219−237.
(42) Wishart, D. S.; Knox, C.; Guo, A. C.; Shrivastava, S.; Hassanali, M.; Stothard, P.; Chang, Z.; Woolsey, J. DrugBank: A Comprehensive Resource for *In Silico* Drug Discovery and Exploration. *Nucleic Acids Res.* **2006**, *34*, D668−72.
(43) Kessel, M.; Gieseler, F.; Woodcock, B. G. Influence of Serum Protein Binding on the Uptake and Retention of Idarubicin by Sensitive and Multidrug Resistant Human Leukemic Cells. *Eur. J. Clin. Pharmacol.* **1999**, *55*, 369−373.
(44) Trainor, G. L. The Importance of Plasma Protein Binding in Drug Discovery. *Expert Opin. Drug Discovery* **2007**, *2*, 51−64.
(45) Schmidt, S.; Röck, K.; Sahre, M.; Burkhardt, O.; Brunner, M.; Lobmeyer, M. T.; Derendorf, H. Effect of Protein Binding on the Pharmacological Activity of Highly Bound Antibiotics. *Antimicrob. Agents Chemother.* **2008**, *52*, 3994−4000.
(46) Kramer, N. I.; Krismartina, M.; Rico-Rico, Á.; Blaauboer, B. J.; Hermens, J. L. M. Quantifying Processes Determining the Free Concentration of Phenanthrene in Basal Cytotoxicity Assays. *Chem. Res. Toxicol.* **2012**, *25*, 436−445.
(47) Ghafourian, T.; Amin, Z. QSAR Models for the Prediction of Plasma Protein Binding. *Bioimpacts* **2013**, *3*, 21−27.
(48) Trapp, S.; Rosania, G. R.; Horobin, R. W.; Kornhuber, J. Quantitative Modeling of Selective Lysosomal Targeting for Drug Design. *Eur. Biophys. J.* **2008**, *37*, 1317−1328.
(49) Ufuk, A.; Somers, G.; Houston, J. B.; Galetin, A. *In Vitro* Assessment of Uptake and Lysosomal Sequestration of Respiratory Drugs in Alveolar Macrophage Cell Line NR8383. *Pharm. Res.* **2015**, *32*, 3937−3951.
(50) van Rensburg, J. J.; Fortney, K. R.; Chen, L.; Krieger, A. J.; Lima, B. P.; Wolfe, A. J.; Katz, B. P.; Zhang, Z.-Y.; Spinola, S. M. Development and Validation of a High-Throughput Cell-Based Screen to Identify Activators of a Bacterial Two-Component Signal Transduction System. *Antimicrob. Agents Chemother.* **2015**, *59*, 3789−3799.
(51) Tsai, C. M.; Perng, R. P.; Chang, K. T.; Venzon, D.; Gazdar, A. F. Evaluation of the Relative Cytotoxic Effects of Anticancer Agents in Serum-Supplemented *versus* Serum-Free Media Using a Tetrazolium Colorimetric Assay. *Jpn. J. Cancer Res.* **1996**, *87*, 91−97.
(52) Schreier, S.; Malheiros, S. V. P.; de Paula, E. Surface Active Drugs: Self-Association and Interaction with Membranes and Surfactants. Physicochemical and Biological Aspects. *Biochim. Biophys. Acta, Biomembr.* **2000**, *1508*, 210−234.
(53) Rhein, C.; Löber, S.; Gmeiner, P.; Gulbins, E.; Tripal, P.; Kornhuber, J. Derivatization of Common Antidepressant Drugs Increases Inhibition of Acid Sphingomyelinase and Reduces Induction of Phospholipidosis. *J. Neural Transm.* **2018**, *125*, 1837−1845.
(54) Skuta, C.; Popr, M.; Muller, T.; Jindrich, J.; Kahle, M.; Sedlak, D.; Svozil, D.; Bartunek, P. Probes & Drugs Portal: An Interactive, Open Data Resource for Chemical Biology. *Nat. Methods* **2017**, *14*, 759−760.
(55) Kornhuber, J.; Tripal, P.; Reichel, M.; Mühle, C.; Rhein, C.; Muehlbacher, M.; Groemer, T. W.; Gulbins, E. Functional Inhibitors of Acid Sphingomyelinase (FIASMAs): A Novel Pharmacological Group of Drugs with Broad Clinical Applications. *Cell. Physiol. Biochem.* **2010**, *26*, 9−20.
(56) Erlich, S.; Miranda, S. R.; Visser, J. W.; Dagan, A.; Gatt, S.; Schuchman, E. H. Fluorescence-Based Selection of Gene-Corrected Hematopoietic Stem and Progenitor Cells from Acid Sphingomyelinase-Deficient Mice: Implications for Niemann-Pick Disease Gene Therapy and the Development of Improved Stem Cell Gene Transfer Procedures. *Blood* **1999**, *93*, 80−86.
(57) Butler, A.; He, X.; Gordon, R. E.; Wu, H.-S.; Gatt, S.; Schuchman, E. H. Reproductive Pathology and Sperm Physiology in Acid Sphingomyelinase-Deficient Mice. *Am. J. Pathol.* **2002**, *161*, 1061−1075.
(58) Manthe, R. L.; Rappaport, J. A.; Long, Y.; Solomon, M.; Veluvolu, V.; Hildreth, M.; Gugutkov, D.; Marugan, J.; Zheng, W.; Muro, S. δ-Tocopherol Effect on Endocytosis and Its Combination with Enzyme Replacement Therapy for Lysosomal Disorders: A New Type of Drug Interaction? *J. Pharmacol. Exp. Ther.* **2019**, *370*, 823−833.
(59) Klutzny, S.; Lesche, R.; Keck, M.; Kaulfuss, S.; Schlicker, A.; Christian, S.; Sperl, C.; Neuhaus, R.; Mowat, J.; Steckel, M.; Riefke, B.; Prechtl, S.; Parczyk, K.; Steigemann, P. Functional Inhibition of Acid Sphingomyelinase by Fluphenazine Triggers Hypoxia-Specific Tumor Cell Death. *Cell Death Dis.* **2017**, *8*, No. e2709.
(60) *JChem for Office (Excel)*, version 17.21.0.1797; ChemAxon: Budapest, Hungary, 2017. Software was used for chemical database access, structure-based property calculation, search, and reporting.
(61) Evers, M. M.; Toonen, L. J. A.; van Roon-Mom, W. M. C. Antisense Oligonucleotides in Therapy for Neurodegenerative Disorders. *Adv. Drug Delivery Rev.* **2015**, *87*, 90−103.
(62) Lieberman, J. Tapping the RNA World for Therapeutics. *Nat. Struct. Mol. Biol.* **2018**, *25*, 357−364.
(63) Schütz, I.; Lopez-Hernandez, T.; Gao, Q.; Puchkov, D.; Jabs, S.; Nordmeyer, D.; Schmudde, M.; Rühl, E.; Graf, C. M.; Haucke, V. Lysosomal Dysfunction Caused by Cellular Accumulation of Silica Nanoparticles. *J. Biol. Chem.* **2016**, *291*, 14170−14184.
(64) Shen, J.; Kim, H.-C.; Su, H.; Wang, F.; Wolfram, J.; Kirui, D.; Mai, J.; Mu, C.; Ji, L.-N.; Mao, Z.-W.; Shen, H. Cyclodextrin and Polyethylenimine Functionalized Mesoporous Silica Nanoparticles for Delivery of SiRNA Cancer Therapeutics. *Theranostics* **2014**, *4*, 487−497.
(65) Wang, M.; Li, X.; Ma, Y.; Gu, H. Endosomal Escape Kinetics of Mesoporous Silica-Based System for Efficient SiRNA Delivery. *Int. J. Pharm.* **2013**, *448*, 51−57.
(66) Bøe, S.; Longva, A. S.; Hovig, E. Photochemically Induced Gene Silencing Using Small Interfering RNA Molecules in Combination with Lipid Carriers. *Oligonucleotides* **2007**, *17*, 166−173.
(67) Xiong, R.; Vandenbroucke, R. E.; Broos, K.; Brans, T.; Van Wonterghem, E.; Libert, C.; Demeester, J.; De Smedt, S. C.; Braeckmans, K. Sizing Nanomaterials in Bio-Fluids by CFRAP Enables

https://dx.doi.org/10.1021/acsnano.0c00666
ACS Nano 2020, 14, 4774−4791

Protein Aggregation Measurements and Diagnosis of Bio-Barrier Permeability. *Nat. Commun.* **2016**, *7*, 12982.
(68) Aits, S.; Jäättelä, M. Lysosomal Cell Death at a Glance. *J. Cell Sci.* **2013**, *126*, 1905−1912.
(69) Gómez-Sintes, R.; Ledesma, M. D.; Boya, P. Lysosomal Cell Death Mechanisms in Aging. *Ageing Res. Rev.* **2016**, *32*, 150−168.
(70) Stoka, V.; Turk, V.; Turk, B. Lysosomal Cathepsins and Their Regulation in Aging and Neurodegeneration. *Ageing Res. Rev.* **2016**, *32*, 22−37.
(71) Papadopoulos, C.; Kravic, B.; Meyer, H. Repair or Lysophagy: Dealing with Damaged Lysosomes. *J. Mol. Biol.* **2020**, *432*, 231−239.
(72) Radulovic, M.; Schink, K. O.; Wenzel, E. M.; Nähse, V.; Bongiovanni, A.; Lafont, F.; Stenmark, H. ESCRT-Mediated Lysosome Repair Precedes Lysophagy and Promotes Cell Survival. *EMBO J.* **2018**, *37*, No. e99753.
(73) Naeye, B.; Deschout, H.; Röding, M.; Rudemo, M.; Delanghe, J.; Devreese, K.; Demeester, J.; Braeckmans, K.; De Smedt, S. C.; Raemdonck, K. Hemocompatibility of SiRNA Loaded Dextran Nanogels. *Biomaterials* **2011**, *32*, 9120−9127.
(74) Remaut, K.; Lucas, B.; Braeckmans, K.; Sanders, N. N.; Demeester, J.; De Smedt, S. C. Protection of Oligonucleotides against Nucleases by Pegylated and Non-Pegylated Liposomes as Studied by Fluorescence Correlation Spectroscopy. *J. Controlled Release* **2005**, *110*, 212−226.
(75) Buyens, K.; Demeester, J.; De Smedt, S. S.; Sanders, N. N. Elucidating the Encapsulation of Short Interfering RNA in PEGylated Cationic Liposomes. *Langmuir* **2009**, *25*, 4886−4891.
(76) Dakwar, G. R.; Zagato, E.; Delanghe, J.; Hobel, S.; Aigner, A.; Denys, H.; Braeckmans, K.; Ceelen, W.; De Smedt, S. C.; Remaut, K. Colloidal Stability of Nano-Sized Particles in the Peritoneal Fluid: Towards Optimizing Drug Delivery Systems for Intraperitoneal Therapy. *Acta Biomater.* **2014**, *10*, 2965−2975.
(77) Buyens, K.; Lucas, B.; Raemdonck, K.; Braeckmans, K.; Vercammen, J.; Hendrix, J.; Engelborghs, Y.; De Smedt, S. C.; Sanders, N. N. A Fast and Sensitive Method for Measuring the Integrity of SiRNA-Carrier Complexes in Full Human Serum. *J. Controlled Release* **2008**, *126*, 67−76.
(78) Shi, F.; Wasungu, L.; Nomden, A.; Stuart, M. C. A.; Polushkin, E.; Engberts, J. B. F. N.; Hoekstra, D. Interference of Poly(Ethylene Glycol)-Lipid Analogues with Cationic-Lipid-Mediated Delivery of Oligonucleotides; Role of Lipid Exchangeability and Non-Lamellar Transitions. *Biochem. J.* **2002**, *366*, 333−341.
(79) Remaut, K.; Lucas, B.; Braeckmans, K.; Demeester, J.; De Smedt, S. C. Pegylation of Liposomes Favours the Endosomal Degradation of the Delivered Phosphodiester Oligonucleotides. *J. Controlled Release* **2007**, *117*, 256−266.
(80) Pedroso de Lima, M. C.; Simões, S.; Pires, P.; Faneca, H.; Düzgüneş, N. Cationic Lipid−DNA Complexes in Gene Delivery: From Biophysics to Biological Applications. *Adv. Drug Delivery Rev.* **2001**, *47*, 277−294.
(81) Zelphati, O.; Szoka, F. C. Cationic Liposomes as an Oligonucleotide Carrier: Mechanism of Action. *J. Liposome Res.* **1997**, *7*, 31−49.
(82) Jyotsana, N.; Sharma, A.; Chaturvedi, A.; Budida, R.; Scherr, M.; Kuchenbauer, F.; Lindner, R.; Noyan, F.; Sühs, K. W.; Stangel, M.; Grote-Koska, D.; Brand, K.; Vornlocher, H. P.; Eder, M.; Thol, F.; Ganser, A.; Humphries, R. K.; Ramsay, E.; Cullis, P.; Heuser, M. Lipid Nanoparticle-Mediated SiRNA Delivery for Safe Targeting of Human CML *In Vivo*. *Ann. Hematol.* **2019**, *98*, 1905−1918.
(83) Kulkarni, J. A.; Darjuan, M. M.; Mercer, J. E.; Chen, S.; van der Meel, R.; Thewalt, J. L.; Tam, Y. Y. C.; Cullis, P. R. On the Formation and Morphology of Lipid Nanoparticles Containing Ionizable Cationic Lipids and SiRNA. *ACS Nano* **2018**, *12*, 4787−4795.
(84) Leung, A. K. K.; Tam, Y. Y. C.; Chen, S.; Hafez, I. M.; Cullis, P. R. Microfluidic Mixing: A General Method for Encapsulating Macromolecules in Lipid Nanoparticle Systems. *J. Phys. Chem. B* **2015**, *119*, 8698−8706.
(85) Wood, H. FDA Approves Patisiran to Treat Hereditary Transthyretin Amyloidosis. *Nat. Rev. Neurol.* **2018**, *14*, 570.
(86) Gould, S. E.; Junttila, M. R.; De Sauvage, F. J. Translational Value of Mouse Models in Oncology Drug Development. *Nat. Med.* **2015**, *21*, 431−439.
(87) Dakwar, G. R.; Braeckmans, K.; Demeester, J.; Ceelen, W.; Smedt, S. C. De; Remaut, K. Disregarded Effect of Biological Fluids in SiRNA Delivery: Human Ascites Fluid Severely Restricts Cellular Uptake of Nanoparticles. *ACS Appl. Mater. Interfaces* **2015**, *7*, 24322−24329.
(88) Gulbins, E.; Kolesnick, R. N. It Takes a CAD to Kill a Tumor Cell with a LMP. *Cancer Cell* **2013**, *24*, 279−281.
(89) Verdoodt, F.; Dehlendorff, C.; Jäättelä, M.; Strauss, R.; Pottegård, A.; Hallas, J.; Friis, S.; Kjaer, S. K. Antihistamines and Ovarian Cancer Survival: Nationwide Cohort Study and *In Vitro* Cell Viability Assay. *JNCI J. Natl. Cancer Inst.* **2019**, *112*, No. djz217.
(90) Boya, P.; Kroemer, G. Lysosomal Membrane Permeabilization in Cell Death. *Oncogene* **2008**, *27*, 6434−6451.
(91) Gulbins, E.; Palmada, M.; Reichel, M.; Lüth, A.; Böhmer, C.; Amato, D.; Müller, C. P.; Tischbirek, C. H.; Groemer, T. W.; Tabatabai, G.; Becker, K. A.; Tripal, P.; Staedtler, S.; Ackermann, T. F.; Van Brederode, J.; Alzheimer, C.; Weller, M.; Lang, U. E.; Kleuser, B.; Grassmé, H.; et al. Acid Sphingomyelinase-Ceramide System Mediates Effects of Antidepressant Drugs. *Nat. Med.* **2013**, *19*, 934−938.
(92) Teichgräber, V.; Ulrich, M.; Endlich, N.; Riethmüller, J.; Wilker, B.; De Oliveira-Munding, C. C.; Van Heeckeren, A. M.; Barr, M. L.; Von Kürthy, G.; Schmid, K. W.; Weller, M.; Tümmler, B.; Lang, F.; Grassme, H.; Döring, G.; Gulbins, E. Ceramide Accumulation Mediates Inflammation, Cell Death and Infection Susceptibility in Cystic Fibrosis. *Nat. Med.* **2008**, *14*, 382−391.
(93) Becker, K. A.; Riethmüller, J.; Lüth, A.; Döring, G.; Kleuser, B.; Gulbins, E. Acid Sphingomyelinase Inhibitors Normalize Pulmonary Ceramide and Inflammation in Cystic Fibrosis. *Am. J. Respir. Cell Mol. Biol.* **2010**, *42*, 716−724.
(94) Becker, K. A.; Riethmüller, J.; Seitz, A. P.; Gardner, A.; Boudreau, R.; Kamler, M.; Kleuser, B.; Schuchman, E.; Caldwell, C. C.; Edwards, M. J.; Grassmé, H.; Brodlie, M.; Gulbins, E. Sphingolipids as Targets for Inhalation Treatment of Cystic Fibrosis. *Adv. Drug Delivery Rev.* **2018**, *133*, 66−75.
(95) Campbell, F.; Bos, F. L.; Sieber, S.; Arias-Alpizar, G.; Koch, B. E.; Huwyler, J.; Kros, A.; Bussmann, J. Directing Nanoparticle Biodistribution through Evasion and Exploitation of Stab2-Dependent Nanoparticle Uptake. *ACS Nano* **2018**, *12*, 2138−2150.
(96) Hayashi, Y.; Takamiya, M.; Jensen, P. B.; Ojea-Jiménez, I.; Claude, H.; Antony, C.; Kjaer-Sorensen, K.; Grabher, C.; Boesen, T.; Gilliland, D.; Oxvig, C.; Strähle, U.; Weiss, C. Differential Nanoparticle Sequestration by Macrophages and Scavenger Endothelial Cells Visualized *In Vivo* in Real-Time and at Ultrastructural Resolution. *ACS Nano* **2020**, *14*, 1665−1681.
(97) Kannan, R.; Sarma, J. S. M.; Guha, M.; Venkataraman, K. Amiodarone Toxicity: II. Desethylamiodarone-Induced Phospholipidosis and Ultrastructural Changes during Repeated Administration in Rats. *Fundam. Appl. Toxicol.* **1991**, *16*, 103−109.
(98) Hostetler, K. Y.; Reasor, M.; Yazaki, P. J. Chloroquine-Induced Phospholipid Fatty Liver, Measurement of Drug and Lipid Concentrations in Rat Liver. *J. Biol. Chem.* **1985**, *260*, 215−219.
(99) Jiang, M.; Huang, S.; Duan, W.; Liu, Q.; Lei, M. Inhibition of Acid Sphingomyelinase Activity Ameliorates Endothelial Dysfunction in Db/Db Mice. *Biosci. Rep.* **2019**, *39*, BSR20182144.
(100) Li, X.; Jin, S. J.; Su, J.; Li, X. X.; Xu, M. Acid Sphingomyelinase Down-Regulation Alleviates Vascular Endothelial Insulin Resistance in Diabetic Rats. *Basic Clin. Pharmacol. Toxicol.* **2018**, *123*, 645−659.
(101) Schiroli, D.; Gómara, M. J.; Maurizi, E.; Atkinson, S. D.; Mairs, L.; Christie, K. A.; Cobice, D. F.; McCrudden, C. M.; Nesbit, M. A.; Haro, I.; Moore, T. Effective *In Vivo* Topical Delivery of SiRNA and Gene Silencing in Intact Corneal Epithelium Using a Modified Cell Penetrating Peptide. *Mol. Ther.–Nucleic Acids* **2019**, *17*, 891−906.
(102) Castanotto, D.; Lin, M.; Kowolik, C.; Wang, L.; Ren, X.-Q.; Soifer, H. S.; Koch, T.; Hansen, B. R.; Oerum, H.; Armstrong, B.; Wang, Z.; Bauer, P.; Rossi, J.; Stein, C. A. A Cytoplasmic Pathway for Gapmer

https://dx.doi.org/10.1021/acsnano.0c00666
ACS Nano 2020, 14, 4774−4791

Antisense Oligonucleotide-Mediated Gene Silencing in Mammalian Cells. *Nucleic Acids Res.* **2015**, *43*, 9350−9361.
(103) Ragelle, H.; Colombo, S.; Pourcelle, V.; Vanvarenberg, K.; Vandermeulen, G.; Bouzin, C.; Marchand-Brynaert, J.; Feron, O.; Foged, C.; Préat, V. Intracellular SiRNA Delivery Dynamics of Integrin-Targeted, PEGylated Chitosan−Poly(Ethylene Imine) Hybrid Nanoparticles: A Mechanistic Insight. *J. Controlled Release* **2015**, *211*, 1−9.
(104) Bramsen, J. B.; Laursen, M. B.; Damgaard, C. K.; Lena, S. W.; Ravindra Babu, B.; Wengel, J.; Kjems, J. Improved Silencing Properties Using Small Internally Segmented Interfering RNAs. *Nucleic Acids Res.* **2007**, *35*, 5886−5897.
(105) Schwabe, K.; Ewe, A.; Kohn, C.; Loth, T.; Aigner, A.; Hacker, M. C.; Schulz-Siegmund, M. Sustained Delivery of SiRNA Poly- and Lipopolyplexes from Porous Macromer-Crosslinked Gelatin Gels. *Int. J. Pharm.* **2017**, *526*, 178−187.
(106) De Vlieghere, E.; Carlier, C.; Ceelen, W.; Bracke, M.; De Wever, O. Data on *In Vivo* Selection of SK-OV-3 Luc Ovarian Cancer Cells and Intraperitoneal Tumor Formation with Low Inoculation Numbers. *Data Br.* **2016**, *6*, 542−549.
(107) Houthaeve, G.; Xiong, R.; Robijns, J.; Luyckx, B.; Beulque, Y.; Brans, T.; Campsteijn, C.; Samal, S. K.; Stremersch, S.; De Smedt, S. C.; Braeckmans, K.; De Vos, W. H. Targeted Perturbation of Nuclear Envelope Integrity with Vapor Nanobubble-Mediated Photoporation. *ACS Nano* **2018**, *12*, 7791−7802.
(108) Fraire, J. C.; Houthaeve, G.; Liu, J.; Raes, L.; Vermeulen, L.; Stremersch, S.; Brans, T.; García-Díaz Barriga, G.; De Keulenaer, S.; Van Nieuwerburgh, F.; De Rycke, R.; Vandesompele, J.; Mestdagh, P.; Raemdonck, K.; De Vos, W. H.; De Smedt, S.; Braeckmans, K. Vapor Nanobubble Is the More Reliable Photothermal Mechanism for Inducing Endosomal Escape of SiRNA without Disturbing Cell Homeostasis. *J. Controlled Release* **2020**, *319*, 262−275.
(109) Rehman, Z. ur; Hoekstra, D.; Zuhorn, I. S. Mechanism of Polyplex- and Lipoplex-Mediated Delivery of Nucleic Acids: Real-Time Visualization of Transient Membrane Destabilization without Endosomal Lysis. *ACS Nano* **2013**, *7*, 3767−3777.
(110) Vermeulen, L. M. P.; Brans, T.; Samal, S. K.; Dubruel, P.; Demeester, J.; De Smedt, S. C.; Remaut, K.; Braeckmans, K. Endosomal Size and Membrane Leakiness Influence Proton Sponge-Based Rupture of Endosomal Vesicles. *ACS Nano* **2018**, *12*, 2332−2345.

https://dx.doi.org/10.1021/acsnano.0c00666
ACS Nano 2020, 14, 4774−4791